



# Analytical modeling and investigation of constrained layer damping in hybrid laminates based on a unified plate formulation

Alexander Jackstadt<sup>a,b,\*</sup>, Wilfried V. Liebig<sup>b</sup>, Luise Kärger<sup>a</sup>

<sup>a</sup> Karlsruhe Institute of Technology (KIT), Institute of Vehicle System Technology (FAST), Lightweight Technology, Rintheimer Querallee 2, 76131 Karlsruhe, Germany

<sup>b</sup> Karlsruhe Institute of Technology (KIT), Institute for Applied Materials (IAM), Materials Science and Engineering, Engelbert-Arnold-Straße 4, 76131 Karlsruhe, Germany

## ARTICLE INFO

### Keywords:

Plates  
Vibration  
Laminate mechanics  
Composites  
Elastomers  
Viscoelasticity

## ABSTRACT

Hybrid laminates, such as fiber metal laminates, are increasingly used in engineering applications due to their outstanding damage tolerance and weight-specific performance. Prone to vibrations, fiber metal laminates have recently been complemented by viscoelastic elastomer layers in order to achieve a desired level of damping following the principles of constrained layer damping. This paper presents an analytical modeling approach based on a unified plate formulation for the rapid and precise analysis of such hybrid laminates regarding their deformation and dynamic behavior. In order to account for the transverse shear deformation in the damping layers, the Reissner's Mixed Variational Theorem is employed. The viscoelastic, thus frequency-dependent, material behavior is taken into account and the resulting damping quantities analyzed. Damped and undamped natural frequencies are computed using an iterative algorithm and the results are compared to the plate's response to forced vibration. The approach is numerically validated using refined finite element models. Additionally, laminate parameters are varied in order to investigate their influence on the damping capabilities of these hybrid laminates.

## 1. Introduction

Because of their outstanding mechanical properties in relation to their low mass density, fiber-reinforced polymers (FRPs), such as CFRPs and glass fiber-reinforced polymers (GFRPs) are widely used in numerous fields such as aerospace and automotive. However, some drawbacks of FRPs include their limited damage tolerance and undesired dynamic behavior when subjected to vibrations. The recent development of fiber metal laminates (FMLs) has been proven effective in increasing the damage tolerance of FRPs by adding metal layers to the lamination scheme. The combination of GFRP and aluminum for example has been widely used in the aviation industry [1]. Nevertheless, FMLs are still prone to vibrations and can thus cause undesired noise or fail prematurely. One possibility of damping lightweight structures is the application of viscoelastic damping materials such as elastomers. Damping can for example be achieved by covering parts of the structure with an adherent viscoelastic layer, which undergoes large shear deformation when the structure is subjected to bending vibrations. This mechanism was first investigated by Oberst and Frankenfeld [2] and is commonly referred to as free layer damping (FLD). Closely related

is the dissipation of energy in a viscoelastic layer constrained between two stiffer layers, first described by Kerwin [3] and consequently called constrained layer damping (CLD). Applications of CLD aimed at the control of vibrations are numerous, and the accompanying research is summarized by Rao [4] and Zhou et al. [5]. One specific class of material systems aimed at the improvement of the dynamic behavior of conventional FMLs are HyCEML. Not only does the elastomer layer provide damping according to the CLD mechanism, but also allows the presence of CFRP and aluminum in one laminate by preventing galvanic corrosion and compensating the mismatch in thermal expansion coefficients [6]. The damping behavior of such laminates has been investigated in previous studies by Liebig et al. [7] and Sessner et al. [8–10]. Similar studies have been conducted on laminates containing steel layers and GFRP by Sarlin et al. [11].

Advances in the accurate and efficient modeling of laminated structures have led to a vast amount of techniques for predicting the structural response of composite and sandwich laminates [12]. Generally, modeling approaches can be classified into ESL, LW and zig-zag formulations [13]. While an ESL approach assumes one homogenized

\* Corresponding author at: Karlsruhe Institute of Technology (KIT), Institute of Vehicle System Technology (FAST), Lightweight Technology, Rintheimer Querallee 2, 76131 Karlsruhe, Germany.

E-mail addresses: [alexander.jackstadt@kit.edu](mailto:alexander.jackstadt@kit.edu) (A. Jackstadt), [wilfried.liebig@kit.edu](mailto:wilfried.liebig@kit.edu) (W.V. Liebig), [luise.kaerger@kit.edu](mailto:luise.kaerger@kit.edu) (L. Kärger).

<https://doi.org/10.1016/j.ijmecsci.2021.106964>

Received 20 August 2021; Received in revised form 19 November 2021; Accepted 22 November 2021

Available online 20 December 2021

0020-7403/© 2021 The Authors. Published by Elsevier Ltd. This is an open access article under the CC BY license (<http://creativecommons.org/licenses/by/4.0/>).

displacement field for all layers, in a LW approach, each layer is described by its own set of field variables. Zig-zag formulations are a combination of ESL and LW approaches, but are not part of the present study due to their prescribed relation between the transverse shear strains of adjacent layers. Since the CLD mechanism requires layers that differ significantly in stiffness, and in this case are relatively thick, their mechanical behavior can rather be compared with sandwich structures than monolithic composite laminates. Thus, a LW description of such CLD laminates appears favorable, as pointed out for sandwich plates by Carrera and Brischetto [14], Wetzal et al. [15] and Kärger et al. [16]. The focus of this work is consequently restricted to mainly LW approaches. Variable kinematics approaches have seen comprehensive research interest in recent years, a commonly used one being the Carrera Unified Formulation (CUF) [17–19]. An extension of the CUF is proposed by Demasi [20–24] referred to as the Generalized Unified Formulation (GUF). Both variable kinematics approaches, CUF and GUF, allow for LW and ESL descriptions as well as theories of arbitrary order. As the optimal theory is highly dependent on the problem at hand, variable kinematics approaches allow for the simple adjustment of a theory in order to achieve the required accuracy with a minimum of variables. This procedure is known as the asymptotic/axiomatic method, investigated among others in [25–28]. The applicability of GUF to the aforementioned HyCEML material has been shown by Jackstadt et al. [29]. A further refinement of the GUF is proposed by D’Ottavio [30] where multiple plies can be treated as an independent sublaminates in a layerwise description, allowing for different models to be used within the same laminate.

A great number of publications deal with the dynamic analysis of composite laminates and sandwich plates. The CUF for example is applied for vibration analysis by Carrera in [31,32]. Further works are omitted for brevity, but comprehensive reviews are given by Qatu et al. [33] and Sayyad et al. [34].

The prediction of the effectiveness of such CLD measures due to viscoelastic layers has been the subject of numerous studies. Early propositions for predictive models include the work of Ross et al. [35] resulting in the commonly used Ross–Kerwin–Ungar (RKU) model. Furthermore, research dealing with the analysis of such viscoelastic laminates using appropriate beam, plate and shell theories. Since this paper focuses on the dynamic response of plates only, works on beams are omitted, although the publications by Rao and He [36], Ganapathi et al. [37], Xi and Shepard [38] and Gupta et al. [39] are worth mentioning. For the prediction of damping in plates with constrained viscoelastic layers, many authors have employed the FEM. Early works include Johnson and Kienholz [40] and Rikards et al. [41]. More recent works utilizing layerwise finite elements for the prediction of the dynamic response of viscoelastic laminates include, but are not limited to, Moreira et al. [42], Plagianakos and Saravanos [43], Akoussan et al. [44] and Ren et al. [45]. The CUF has also been used in said context by Filippi et al. [46] and Ribeiro et al. [47]. In addition to the FEM, analytical procedures such as the Navier method [12] have also been employed to analyze the damping capabilities of viscoelastic laminates. Saravanos and Pereira [48] determine the frequency response and modal damping parameters of simply supported composite plates with interlaminar damping layers using a discrete-layer laminate theory. An optimization procedure to increase the damping loss factor of plates under general edge conditions is presented by Li and Narita [49]. Alaimo et al. [50] determine the free vibration and forced vibration response of plates and use a fractional derivatives approach for representing the viscoelastic layers in frequency domain. The work of Valvano et al. [51] focuses on the sound transmission of shells including viscoelastic damping layers. Different types of loading are considered. Wang et al. [52] use an analytical model to predict the natural frequencies and modal loss factors of co-cured composite plates incorporating damping membranes using a first-order zig-zag theory. Li et al. [53] study the nonlinear vibration behavior of cylindrical shells with partial CLD treatment with the help of an analytical model and

**Table 1**

Linear elastic material parameters of CFRP under the assumption of transverse isotropy.

$E_1$ in GPa	$E_2$ in GPa	$\nu_{12}$	$G_{12}$ in GPa	$G_{23}$ in GPa
108.70	7.70	0.34	3.76	2.75

**Table 2**

Linear elastic material parameters of aluminum sheet metal.

$E$ in GPa	$\nu$
73.10	0.30

find the achievable damping ratios to be dependent on the excitation amplitudes. Li et al. [54] also study the adaptive vibrational behavior of plates with magnetorheological elastomer damping layers. Jackstadt and Kärger [55] apply the GUF based on mixed variational theorem to determine the forced vibration response of simple isotropic CLD laminates. The sublaminates based GUF [30] is employed by D’Ottavio et al. [56] to identify frequency response, modal loss factors and damped natural frequencies of a variety of laminates incorporating viscoelastic damping layers.

This paper presents an analytical approach for the dynamic analysis of hybrid CFRP elastomer metal laminates. To the authors’ knowledge, the Reissner’s Mixed Variational Theorem (RMVT) in conjunction with the complex modulus approach and the GUF framework are used for the first time for the analysis of viscoelastic CLD laminates. In order to reduce computational effort, the required degrees of freedom (DOF) are reduced by employing a combined hybrid LW and ESL approach similar to the sublaminates GUF published in [30]. Specifically, the aforementioned HyCEML is investigated regarding its damping capabilities. The analytical approach is verified by comparison with detailed 3D finite element (FE) simulations. Finally, the influence of variations in layer thickness and elastic properties of the damping material is examined making a contribution to the deeper understanding of this intrinsic damping mechanism.

## 2. Materials

The HyCEML material class investigated in this study consists of three individual constituents which are presented in the following. The unidirectional CFRP plies represent the epoxy based prepreg material HexPly M77/38/UD150/CHS-12K-70 by Hexcel. The material is assumed to behave transversely isotropic with the linear elastic properties listed in Table 1. Although the CFRP does show viscoelastic effects, which have been studied in [7], those are neglected in this study. This is justified by the fact that in the considered frequency range, the loss factor  $\tan(\delta)$  of the CFRP is lower by magnitudes than the loss factor of the elastomer material as shown by Sessner [57] and is therefore negligible. The CFRP’s mass density is specified with  $\rho_{\text{CFRP}} = 1480 \text{ kg/m}^3$ .

The aluminum modeled in this study is based on EN AW-2024 T3 ALCLAD AMS-QQA-250/5 alloy sheets. The linear elastic properties are listed in Table 2 and its mass density taken as  $\rho_{\text{Al}} = 2780 \text{ kg/m}^3$ . The viscoelastic damping layers in the HyCEML considered here consist of an ethylene propylene diene monomer (EPDM) rubber SAA9579-52 by Gummiwerk KRAIBURG GmbH & Co. KG. The mass density is given by  $\rho_{\text{EPDM}} = 1180 \text{ kg/m}^3$ . The viscoelastic, thus frequency-dependent, properties of this material in terms of its complex shear modulus

$$G^* = \Re(G^*) + i\Im(G^*) = G' + iG'' = G^*(\omega) \quad (1)$$

are shown in Fig. 1. The real part of the complex shear modulus  $\Re(G^*) = G'$  is referred to as the storage modulus and represents the elastic part of the mechanical behavior, whereas the imaginary part  $\Im(G^*) = G''$  is the loss modulus and describes the dissipative or viscous contribution. A measure for the material damping is given by the loss factor  $\tan(\delta) = G''/G'$ .

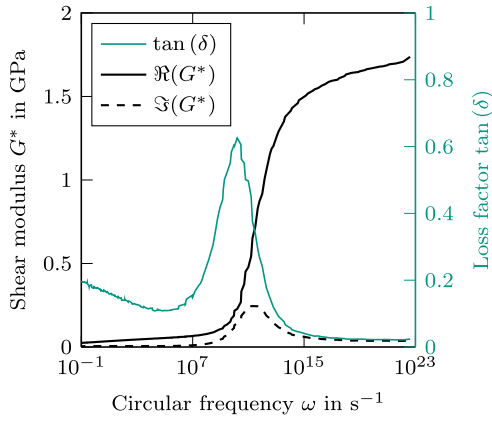


Fig. 1. Complex shear modulus  $G^*$  and loss factor  $\tan(\delta)$  over frequency of the elastomer material. The data has been determined in a torsion rheometer test.

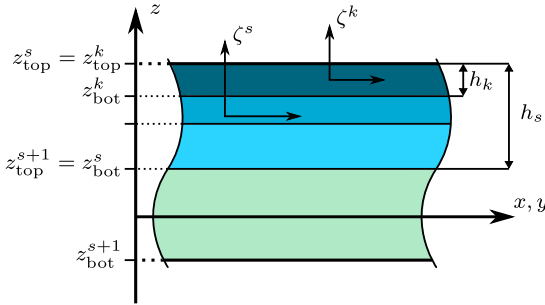


Fig. 2. Laminate coordinate system showing two sublaminae  $s$  (blue) and  $s+1$  (green). Layer  $s$  consists of multiple material layers of which an arbitrary one,  $k$ , is shown as an example. (For interpretation of the references to color in this figure legend, the reader is referred to the web version of this article.)

### 3. Modeling approach

#### 3.1. Description of the laminated plate in thickness direction

The description of the laminated plate in thickness direction is illustrated in Fig. 14. The global thickness coordinate is  $z$ . The plate consists of an arbitrary number of material plies with individual thicknesses  $h_k$ , which are assumed to have ideal adhesion. For each material layer  $k$  the dimensionless coordinate

$$\zeta^k = \frac{2}{z_{\text{top}}^k - z_{\text{bot}}^k} z - \frac{z_{\text{top}}^k + z_{\text{bot}}^k}{z_{\text{top}}^k - z_{\text{bot}}^k} \quad (2)$$

is defined so that  $\zeta^k(z_{\text{top}}^k) = 1$  and  $\zeta^k(z_{\text{bot}}^k) = -1$ , where  $z_{\text{top}}^k$  and  $z_{\text{bot}}^k$  are the upper and lower interfaces of ply  $k$  in the global coordinate  $z$ . Each material ply  $k$  is thus described by its coordinates  $[z_{\text{top}}^k, z_{\text{bot}}^k]$  and its own constitutive matrix (Eq. (5) in Section 3.3). Furthermore, the laminated plate is partitioned into sublaminae. Each sublaminate  $s$  consists of one or more material layers  $k$ . Again, a dimensionless coordinate is introduced as

$$\zeta^s = \frac{2}{z_{\text{top}}^s - z_{\text{bot}}^s} z - \frac{z_{\text{top}}^s + z_{\text{bot}}^s}{z_{\text{top}}^s - z_{\text{bot}}^s} \quad (3)$$

with  $z_{\text{top}}^s$  and  $z_{\text{bot}}^s$  being the upper and lower interface of the sublaminate  $s$  in global coordinates.

#### 3.2. Variational principle

Due to the fact that the CLD in laminates is driven by transverse shear stresses within the viscoelastic layers, the Reissner's Mixed Variational Theorem [58] is used as the basis of this work since it allows

for the explicit modeling of out-of-plane stresses. Furthermore, the considered viscoelastic damping layers in the HyCEML class of materials are comparably thick. Both aspects have previously been addressed by Carrera [32] and the use of a mixed variational principle has been encouraged. The RMVT in the dynamic case is herein written as

$$\int_{\Omega} \left( \delta \epsilon_{\text{pG}}^{\text{T}} \sigma_{\text{pH}} + \delta \epsilon_{\text{nG}}^{\text{T}} \sigma_{\text{nM}} + \delta \sigma_{\text{nM}}^{\text{T}} (\epsilon_{\text{nG}} - \epsilon_{\text{nH}}) \right) dV + \int_{\Omega} \rho \delta \mathbf{u}^{\text{T}} \ddot{\mathbf{u}} dV = \delta L_{\text{external}} \quad (4)$$

In Eq. (4), in-plane quantities are denoted by the index  $p$  whereas out-of-plane quantities are indexed with  $n$ . By using a modified Voigt notation, the two vectors containing the infinitesimal strains are  $\epsilon_{\text{p}} = (\epsilon_{xx} \ \epsilon_{yy} \ \gamma_{xy})^{\text{T}}$  and  $\epsilon_{\text{n}} = (\gamma_{xz} \ \gamma_{yz} \ \epsilon_{zz})^{\text{T}}$ . Consequently, the stress vectors  $\sigma_{\text{p}} = (\sigma_{xx} \ \sigma_{yy} \ \sigma_{xy})^{\text{T}}$  and  $\sigma_{\text{n}} = (\sigma_{xz} \ \sigma_{yz} \ \sigma_{zz})^{\text{T}}$  are used. Stress quantities for which an explicit modeling approach is chosen are marked by the index  $M$ . Strain components with the index  $G$  are directly derived from the displacement field  $\mathbf{u}$  using standard geometric relations. The index  $H$  indicates that the quantity is calculated from the mixed form of Hooke's law introduced below in Section 3.3. On the right-hand side of Eq. (4) the virtual variation of work  $\delta L_{\text{external}}$  performed by external loads and the inertia term containing the acceleration  $\ddot{\mathbf{u}}$  are added.

#### 3.3. Constitutive relations

Resulting from the mixed nature of the variational statement in Eq. (4), a mixed form of Hooke's law

$$\begin{Bmatrix} \sigma_{\text{p}} \\ \epsilon_{\text{n}} \end{Bmatrix} = \begin{Bmatrix} C_{\text{pp}} & C_{\text{pn}} \\ C_{\text{np}} & C_{\text{nn}} \end{Bmatrix} \begin{Bmatrix} \epsilon_{\text{p}} \\ \sigma_{\text{n}} \end{Bmatrix} \quad (5)$$

is used to describe the linear elastic and frequency domain viscoelastic behavior. Eq. (5) is derived from the classic form of Hooke's Law as outlined in Appendix A. A comprehensive deduction can also be found in [20]. For a viscoelastic material in frequency domain, the stiffness matrix  $C$  in Eq. (5) becomes complex valued and is calculated from the material's Poisson ratio  $\nu$  and the complex shear modulus  $G^*(\omega)$  in Eq. (1). By using the two complex valued Lamé constants

$$\begin{aligned} \mu^* &= G^* \\ \lambda^* &= \frac{2G^* \nu}{1 - 2\nu} \end{aligned} \quad (6)$$

the stiffness tensor  $C_{ijkl}^* = \lambda^* \delta_{ij} \delta_{kl} + \mu^* (\delta_{ik} \delta_{jl} + \delta_{il} \delta_{jk})$  is calculated and transformed into the mixed form in Eq. (5) according to the relations Appendix A.

#### 3.4. Laminate kinematics and assembly in thickness direction

A modeling approach according to the GUF [20,21] for the three displacement components and the three out-of-plane stress components is used. First, a layerwise description is used for each material layer  $k$ :

$$\begin{aligned} u_x^k(x, y, z) &= U_{x, \alpha u_x}^k F_{\alpha u_x}(z) \Phi_{u_x}(x, y) \\ u_y^k(x, y, z) &= U_{y, \alpha u_y}^k F_{\alpha u_y}(z) \Phi_{u_y}(x, y) \\ u_z^k(x, y, z) &= U_{z, \alpha u_z}^k F_{\alpha u_z}(z) \Phi_{u_z}(x, y) \\ \sigma_{xz}^k(x, y, z) &= S_{xz, \alpha \sigma_{xz}}^k F_{\alpha \sigma_{xz}}(z) \Phi_{\sigma_{xz}}(x, y) \\ \sigma_{yz}^k(x, y, z) &= S_{yz, \alpha \sigma_{yz}}^k F_{\alpha \sigma_{yz}}(z) \Phi_{\sigma_{yz}}(x, y) \\ \sigma_{zz}^k(x, y, z) &= S_{zz, \alpha \sigma_{zz}}^k F_{\alpha \sigma_{zz}}(z) \Phi_{\sigma_{zz}}(x, y) \end{aligned} \quad (7)$$

In Eq. (7), the indices  $\alpha$  are summation indices according to Einstein's summation convention. For each displacement or out-of-plane stress component, the order of expansion is chosen individually. Each index  $\alpha$  then runs from 1 to  $N+1$  indicating that a specific layer displacement or out-of-plane stress component is modeled with  $N+1$  so far unknown

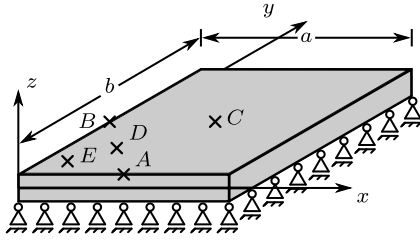


Fig. 3. Simply supported plate with points A, B, C, D and E at which the solution is evaluated.

variables  $U_{i,\alpha_{ij}}^k$  and  $S_{iz,\alpha_{iz}}^k$  respectively. The functions used to expand displacement and out-of-plane stress components  $F_{\alpha_{ij}}(z)$  and  $F_{\alpha_{iz}}(z)$  are combinations of Legendre polynomials and defined as

$$\begin{aligned} F_1 &= \frac{P_0 + P_1}{2} \\ F_m &= P_m - P_{m-2}, \quad m = 2, 3 \dots N \\ F_{N+1} &= \frac{P_0 - P_1}{2} \end{aligned} \quad (8)$$

where  $P_n(\zeta_k)$  are the Legendre polynomials of order  $n = 0..N$ . The in-plane dependencies of the solution are summarized in the functions  $\Phi(x, y)$  and will be addressed in the following section.

### 3.5. Formulation of governing equations for a simply supported plate

In this study, simply supported laminated plates according to Fig. 3 are considered and evaluated regarding their damping behavior. The plate has the in-plane dimensions  $a$  and  $b$  in  $x$ - and  $y$ -direction. An exact Navier-type solution [12] satisfying the boundary conditions shown in Fig. 3 can be obtained when the following three trigonometric distributions for displacements and out-of-plane stresses are assumed:

$$\begin{aligned} \Phi_x &:= \Phi_{u_x}(x, y) = \Phi_{\sigma_{xz}}(x, y) = \cos\left(\frac{m\pi x}{a}\right) \sin\left(\frac{n\pi y}{b}\right) \\ \Phi_y &:= \Phi_{u_y}(x, y) = \Phi_{\sigma_{yz}}(x, y) = \sin\left(\frac{m\pi x}{a}\right) \cos\left(\frac{n\pi y}{b}\right) \\ \Phi_z &:= \Phi_{u_z}(x, y) = \Phi_{\sigma_{zz}}(x, y) = \sin\left(\frac{m\pi x}{a}\right) \sin\left(\frac{n\pi y}{b}\right). \end{aligned} \quad (9)$$

The parameters  $m$  and  $n$  in Eq. (9) correspond to the number of half waves in  $x$ - and  $y$ -direction across the plate. The loads acting on the plate are defined accordingly. In the following, the loads are restricted to those acting perpendicular to the  $x, y$ -plane on a layer  $k$ 's top or bottom surface and are expressed by

$$q_z^{k,\text{top}}(x, y) = \Phi_z Q_z^{k,\text{top}} \quad (10)$$

and

$$q_z^{k,\text{bot}}(x, y) = \Phi_z Q_z^{k,\text{bot}} \quad (11)$$

where  $Q_{z,mn}^{k,\text{top}}$  and  $Q_{z,mn}^{k,\text{bot}}$  are generic pressure load coefficients defined later. In-plane loads are not within the scope of this paper, but can be treated accordingly as shown in Appendix C.

The governing equations for each layer  $k$  are then derived by inserting the approximations for displacements  $u_i^k$  and out-of-plane stresses  $\sigma_{iz}^k$  stated in Eq. (7) into the RMVT in Eq. (4). The layerwise governing equations are listed in Appendix B. In accordance with GUF, 13 stiffness kernel matrices are obtained for each layer  $k$  and are listed in Appendix C. Further details are omitted for reasons of brevity, but the reader is referred to the original publication by Demasi [20] for a complete deduction. Furthermore, the dynamic analyses require the definition of a mass matrix according to the inertia term in Eq. (4). The corresponding mass kernel matrices  $\mathbf{M}_{U_i U_j}^k$  are deduced according to the GUF framework and can also be found in Appendix C alongside the resulting loads  $\mathbf{R}_i^k$ .

Following the expansion of the 13 stiffness kernels in each layer  $k$ , the sublaminates  $s$ , as illustrated in Section 3.1 and Fig. 2, are assembled. This is done according to the ESL assembly procedure outlined in [22]. Thus, the displacement DOF follow an ESL description while out-of-plane stress DOF preserve their layerwise nature and the equilibrium at the interface is imposed. This leads to the global governing equations

$$\begin{aligned} \mathbf{K}_{U_x U_x} \mathbf{U}_x + \mathbf{K}_{U_x U_y} \mathbf{U}_y + \mathbf{K}_{U_x S_x} \mathbf{S}_x + \mathbf{K}_{U_x S_z} \mathbf{S}_z + \mathbf{M}_{U_x U_x} \ddot{\mathbf{U}}_x &= \mathbf{R}_x \\ \mathbf{K}_{U_y U_x} \mathbf{U}_x + \mathbf{K}_{U_y U_y} \mathbf{U}_y + \mathbf{K}_{U_y S_x} \mathbf{S}_x + \mathbf{K}_{U_y S_z} \mathbf{S}_z + \mathbf{M}_{U_y U_y} \ddot{\mathbf{U}}_y &= \mathbf{R}_y \\ \mathbf{K}_{U_z S_x} \mathbf{S}_x + \mathbf{K}_{U_z S_y} \mathbf{S}_y + \mathbf{K}_{U_z S_z} \mathbf{S}_z + \mathbf{M}_{U_z U_z} \ddot{\mathbf{U}}_z &= \mathbf{R}_z \\ \mathbf{K}_{S_x U_x} \mathbf{U}_x + \mathbf{K}_{S_x U_z} \mathbf{U}_z + \mathbf{K}_{S_x S_x} \mathbf{S}_x &= \mathbf{0} \\ \mathbf{K}_{S_y U_y} \mathbf{U}_y + \mathbf{K}_{S_y U_z} \mathbf{U}_z + \mathbf{K}_{S_y S_y} \mathbf{S}_y &= \mathbf{0} \\ \mathbf{K}_{S_z U_x} \mathbf{U}_x + \mathbf{K}_{S_z U_y} \mathbf{U}_y + \mathbf{K}_{S_z U_z} \mathbf{U}_z + \mathbf{K}_{S_z S_z} \mathbf{S}_z &= \mathbf{0} \end{aligned} \quad (12)$$

of the simply supported plate. The vector containing all displacement and out-of-plane DOF will in the following be denoted by  $\mathbf{U} = (\mathbf{U}_x \ \mathbf{U}_y \ \mathbf{U}_z \ \mathbf{S}_x \ \mathbf{S}_y \ \mathbf{S}_z)^\top$  so that the global system of equations in Eq. (12) can be written as

$$\mathbf{K}\mathbf{U} = \mathbf{R} - \mathbf{M}\ddot{\mathbf{U}}. \quad (13)$$

### 3.6. Loading conditions and solution

In the course of this study, three loading conditions are considered for the simply supported laminated plate. First, static loading is applied in order to verify and evaluate the kinematic modeling approach and the combined ESL and LW assembly procedure. These analyses are also used to determine the most suitable theory in terms of order of expansion for the subsequent dynamic analyses, which intend to give a deeper insight into the damping capabilities of the HyCEML material.

#### 3.6.1. Static loading

A sinusoidally distributed pressure load on the top surface ( $k = 1$ ) of the plate is applied. The load coefficient in Eq. (10) then equals the maximum pressure  $\bar{p}$  in the center of plate and the load distribution is the following:

$$q_z^{1,\text{top}}(x, y) = \Phi_z Q_z^{1,\text{top}} = \sin\left(\frac{m\pi x}{a}\right) \sin\left(\frac{n\pi y}{b}\right) \bar{p} \quad (14)$$

Due to the absence of inertia in static loading, the system of equations becomes

$$\mathbf{K}\mathbf{U} = \mathbf{R} \quad (15)$$

and will be solved for the generalized displacement vector  $\mathbf{U}$  containing all DOF. The resulting displacement and stress fields are calculated using Eqs. (7) and (5).

#### 3.6.2. Free vibration

The natural frequencies, corresponding mode shapes and modal damping ratios of the plates are determined under free vibration. In absence of any external loads and the assumption of a harmonic displacement field  $\mathbf{u}(x, y, z, t) = e^{i\omega t} \hat{\mathbf{u}}(x, y, z) = e^{i\omega t} \hat{\mathbf{U}}(z) \Phi(x, y)$  the system of equations becomes

$$(\mathbf{K}_{mn}^* - \lambda_{mn}^* \mathbf{M}_{mn}) \hat{\mathbf{U}}_{mn}^* = \mathbf{0} \quad (16)$$

and is solved for its complex eigenvalues  $\lambda^*$  for each mode shape  $(m, n)$ . Quantities which represent an amplitude of a harmonic oscillation with regard to time are marked with  $\hat{(\cdot)}$ . The stiffness and mass matrices in this case vary with  $m$  and  $n$  as the corresponding kernels in Appendix C are dependent on the functions  $\Phi_x$ ,  $\Phi_y$  and  $\Phi_z$  in Eq. (9). The damped angular natural frequency is calculated as

$$\omega_{mn} = \sqrt{\Re(\lambda_{mn}^*)}. \quad (17)$$

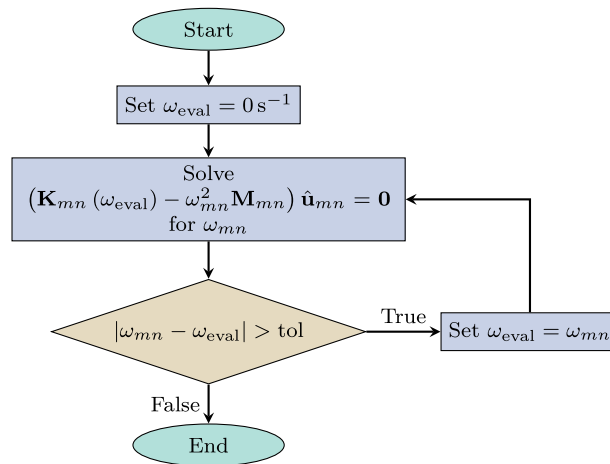


Fig. 4. Flow chart of the iterative eigenvalue solver used for the calculation of natural frequencies.

Table 3

HyCEML layup with layer index  $k$  from top to bottom, rotations  $\theta_k$ , layer thicknesses  $t_k$  and sublaminates index  $s$  for layerwise (LW), equivalent single layer (ESL) and sublaminates (Sub) approaches.

Material	k	$\theta_k$ in deg	$t_k$ in mm	$s_{LW}$	$s_{ESL}$	$s_{Sub}$
CFRP	1	0	0.15	1	1	1
CFRP	2	90	0.15	2	1	1
CFRP	3	90	0.15	3	1	1
CFRP	4	0	0.15	4	1	1
Elastomer	5	0	0.50	5	1	2
Aluminum	6	0	0.30	6	1	3
Elastomer	7	0	0.50	7	1	4
CFRP	8	0	0.15	8	1	5
CFRP	9	90	0.15	9	1	5
CFRP	10	90	0.15	10	1	5
CFRP	11	0	0.15	11	1	5

The modal damping property of the structure is analyzed on the basis of the modal damping ratio

$$\xi_{mn} = \frac{\Im(\lambda_{mn}^*)}{\Re(\lambda_{mn}^*)}. \quad (18)$$

In order to account for the frequency-dependent viscoelastic material behavior of the elastomer layers, an iterative algorithm similar to the one used in [56] is used to approximate the eigenvalues in Eq. (16). The algorithm as implemented is outlined in Fig. 4. Due to reasons of readability, the undamped variant of Eq. (16) is shown, but the procedure remains identical for the damped case with complex stiffness matrix and eigenvalues. The angular frequency at which the viscoelastic material behavior as shown in Fig. 1 is evaluated is denoted as  $\omega_{eval}$ . In this study, the tolerated absolute deviation of evaluation frequency  $\omega_{eval}$  and natural frequency  $\omega_{mn}$  was chosen as  $tol = 1 \times 10^{-3} \text{ s}^{-1}$ .

### 3.6.3. Forced vibration

Forced vibration analysis is used to determine the complex valued frequency response functions (FRFs) of HyCEML plates. Harmonic point loads are considered in this study. While no exact solution exists for these loads and the assumed plate problem, the Navier method [12] is used to superimpose a number of exact solutions of the Navier type seen in Eqs. (7) and (9) in order to approximate the solution. A double trigonometric series is used to express the resulting surface load

$$q_z^{1,top}(x, y, t) = \sum_{m=1}^{\infty} \sum_{n=1}^{\infty} \hat{Q}_{mn} e^{i\omega t} \approx \sum_{m=1}^M \sum_{n=1}^N \hat{Q}_{mn} e^{i\omega t}, \quad (19)$$

where the load coefficient

$$\hat{Q}_{mn} = \frac{4\hat{F}_0}{ab} \Phi_z(x = x_0, y = y_0) \quad (20)$$

depends on  $m$  and  $n$  according to Eq. (9). The coordinates where the concentrated force  $F_0 = \hat{F}_0 e^{i\omega t}$  is applied are denoted with  $x_0$  and  $y_0$ . A concentrated force could be depicted exactly by Eq. (20) if the series was expanded towards infinity. In this study however, a cut-off  $M$  respectively  $N$  is defined. Reasonable values for  $M$  and  $N$  have been investigated in [50,55]. For each value of  $m$  and  $n$  the system of equations

$$(\mathbf{K}_{mn}^* - \omega^2 \mathbf{M}_{mn}) \hat{\mathbf{U}}_{mn}^* = \hat{\mathbf{R}}_{mn} \quad (21)$$

is solved. The corresponding layerwise displacement and stress fields are superimposed accordingly by

$$\begin{aligned} u_x^{*k}(x, y, z, t) &= \sum_{m=1}^M \sum_{n=1}^N \hat{U}_{x,\alpha_{uz}}^{*k,mn} F_{\alpha_{uz}}(z) \Phi_{u_x}(x, y, m, n) e^{i\omega t} \\ u_y^{*k}(x, y, z, t) &= \sum_{m=1}^M \sum_{n=1}^N \hat{U}_{y,\alpha_{uy}}^{*k,mn} F_{\alpha_{uy}}(z) \Phi_{u_y}(x, y, m, n) e^{i\omega t} \\ u_z^{*k}(x, y, z, t) &= \sum_{m=1}^M \sum_{n=1}^N \hat{U}_{z,\alpha_{uz}}^{*k,mn} F_{\alpha_{uz}}(z) \Phi_{u_z}(x, y, m, n) e^{i\omega t} \\ \sigma_{xz}^{*k}(x, y, z, t) &= \sum_{m=1}^M \sum_{n=1}^N \hat{S}_{xz,\alpha_{\sigma_{xz}}}^{*k,mn} F_{\alpha_{\sigma_{xz}}}(z) \Phi_{\sigma_{xz}}(x, y, m, n) e^{i\omega t} \\ \sigma_{yz}^{*k}(x, y, z, t) &= \sum_{m=1}^M \sum_{n=1}^N \hat{S}_{yz,\alpha_{\sigma_{yz}}}^{*k,mn} F_{\alpha_{\sigma_{yz}}}(z) \Phi_{\sigma_{yz}}(x, y, m, n) e^{i\omega t} \\ \sigma_{zz}^{*k}(x, y, z, t) &= \sum_{m=1}^M \sum_{n=1}^N \hat{S}_{zz,\alpha_{\sigma_{zz}}}^{*k,mn} F_{\alpha_{\sigma_{zz}}}(z) \Phi_{\sigma_{zz}}(x, y, m, n) e^{i\omega t}. \end{aligned} \quad (22)$$

For the forced vibration analysis, the frequency range of interest is discretized, and the above solution is calculated on each frequency point. It should be noted that due to the assumed loss factor damping, the above quantities are complex valued and frequency-dependent.

## 4. Model verification and application to HyCEML

The modeling approach illustrated above is implemented in comprehensive Python 3.7.4 code. A plate as shown in Fig. 3 with the dimensions  $a = b = 0.1 \text{ m}$  consisting of the laminate layup shown in Table 3 resulting in an overall laminate thickness  $t = 2.5 \text{ mm}$  is investigated hereafter.

Field variables are evaluated at any of the points listed in Table 4.

In the following, static loading, free vibration and forced vibration are considered.

**Table 4**  
Evaluation points on the simply supported plate from Fig. 3.

Point	A	B	C	D	E
x	0.5a	0.0	0.5a	0.25a	0.125a
y	0.0	0.5b	0.5b	0.25b	0.125b

**Table 5**  
Full layerwise theories with different order of expansions for displacements  $u_i$  and out-of-plane stresses  $\sigma_{iz}$ .

Name	$N_{u_x}$	$N_{u_y}$	$N_{u_z}$	$N_{\sigma_{xz}}$	$N_{\sigma_{yz}}$	$N_{\sigma_{zz}}$
LW <sub>111</sub> <sup>111</sup>	1	1	1	1	1	1
LW <sub>112</sub> <sup>223</sup>	1	1	2	2	2	3
LW <sub>333</sub> <sup>335</sup>	3	3	3	5	5	5

#### 4.1. Static loading

Hereafter, a statically loaded plate is analyzed in order to assess the suitability and verify the analytical approach used further on in the dynamic studies. The plate is subjected to a sinusoidal pressure load according to  $m = n = 1$  in Eq. (14) with an amplitude  $\bar{p} = 1$  MPa. The resulting field quantities are evaluated as through-thickness distributions at the points  $A = (a/2|0)$ ,  $B = (0|b/2)$  and  $C = (a/2|b/2)$  shown in Fig. 3 and Table 4.

##### 4.1.1. Investigation of higher-order theories

First, full layerwise theories are investigated and compared to a 3D FEM solution. The FEM solutions presented in this paper have all been obtained using the commercial software package Abaqus/Standard 2020 employing a converged mesh of quadratic continuum elements. The investigated theories used to obtain analytical solutions are summarized in Table 5. Layerwise theories are named LW <sub>$N_{u_x} N_{u_y} N_{u_z}$</sub>  <sup>$N_{\sigma_{xz}} N_{\sigma_{yz}} N_{\sigma_{zz}}$</sup>  with the bottom indices defining the orders of expansion for the displacement components and the top indices specifying the expansions of out-of-plane stresses. Theory LW<sub>111</sub><sup>111</sup> is a layerwise theory of first order, thus representing the least DOF. The higher order theory LW<sub>333</sub><sup>555</sup> is shown here as a convergence limit, as an increase in the orders of expansion does not improve the quality of the solution as previously shown in [29]. A natural choice is theory LW<sub>112</sub><sup>223</sup> which assumed a linear distribution of in-plane displacements and a quadratic one for the displacement component  $u_z$  and the transverse shear stresses  $\sigma_{xz}$  and  $\sigma_{yz}$ . Consequently, a cubic expansion is chosen for the transverse normal stress component  $\sigma_{zz}$ .

##### 4.1.2. Investigation of the sublaminar approach

In this part, the influence of a further reduction of the DOF used in the analytical modeling approach using sublaminar kinematics is assessed. The previously analyzed fully layerwise theory LW<sub>112</sub><sup>223</sup> is used as a reference. It will be compared to an equivalent-single-layer theory of the same order, namely ESL<sub>112</sub><sup>223</sup> in which all material layers share the same displacement DOF and are thus homogenized over the thickness. A sublaminar approach, henceforth named Sub<sub>112</sub><sup>223</sup> is also considered. The theories are named analogously to the layerwise theories with regard to the indices representing the orders of expansion for displacements and out-of-plane stresses. Table 3 summarizes how the laminate is assembled according to the procedure outlined in Section 3.5. In the case of Sub<sub>112</sub><sup>223</sup>, the top CFRP layers as well as the bottom CFRP layers are treated as two equivalent-single-layers due to their similar mechanical properties when compared to the other laminate constituents. The resulting theory equals a layerwise theory with five layers of which two are sublaminates containing the CFRP layers.

#### 4.2. Free vibration

The dynamic behavior of HyCEML is first analyzed under free vibration. In this case, a larger plate with the dimensions  $a = b = 0.4$  m is considered. The boundary conditions remain identical to those shown in Fig. 3. No external loads are present so the plate is allowed to vibrate freely and 25 mode shapes are identified with regard to their undamped and damped natural frequency. The iterative algorithm outlined in Section 3.6.2 to account for frequency-dependent material behavior is compared against the state-of-the-art approach, which does not consider the frequency dependency of the constitutive law. A comparison with results obtained with the FEM using Abaqus/Standard is also presented.

In order to further investigate the CLD mechanism, a parametric study is conducted. First, the stiffness of the elastomer damping layers is varied. The complex shear modulus  $G^*$  is scaled so that a scaled modulus  $\tilde{G}^* = \kappa G^*$  is used in the HyCEML layup investigated before under free vibration. This ensures that the actual loss factor of the material itself remains constant. The complex shear modulus is scaled in the range 0.1 to 10. Additionally, the influence of the elastomer layer thickness  $h_{E1}$  on the free vibration behavior is analyzed. The layer thickness is varied in the range of 0.1 mm to 1.5 mm. Apart from this, the laminate layup remains identical.

#### 4.3. Forced vibration

Forced vibration analysis is used to determine the material's frequency response to a harmonic excitation. The HyCEML plate is excited by a harmonic point load in  $z$ -direction with an amplitude of  $\hat{F}_0 = 10$  N. An excitation frequency range of 1 Hz to 1500 Hz is considered. An expansion order of  $M = N = 64$  for the Navier method is applied here. In order to capture the modes determined in free vibration, three different excitation points are considered, namely point  $C$ ,  $D$  and  $E$  on the simply supported plate shown in Fig. 3. The resulting displacement magnitude  $\|\hat{u}_z^*\|$  and phase angle  $\delta = \arctan2(\Im(u_3^*)/\Re(u_3^*))$  are evaluated and analyzed. A verification of this procedure on a simplified laminate has been published by the authors in [55].

### 5. Results and discussion

#### 5.1. Static loading

In the following, the through-thickness predictions of three full layerwise theories are assessed compared to a 3D FEM prediction. The results for the three displacement components  $u_x$ ,  $u_y$  and  $u_z$  are shown in Fig. 5. It can be seen that all full layerwise theories yield identical results for the in-plane displacements  $u_x$  and  $u_y$ . Due to the layerwise theory, a linear approach for these components seems to suffice and will thus be used in the remainder of investigations in this paper. In the case of the transverse displacement component  $u_z$  a slight deviation between the FEM reference prediction and the analytical predictions of all theories is observed.

The distributions of the normal stresses  $\sigma_{xx}$ ,  $\sigma_{yy}$  and  $\sigma_{zz}$  are shown in Fig. 6. The two in-plane normal stresses have been calculated from the constitutive law Eq. (5) and the displacement field, while the stress  $\sigma_{zz}$  is integrated from the equilibrium conditions. The reader is referred to [29] for details on this procedure. All theories under investigation yield identical results to the FEM reference solution in this case.

Based on the results obtained so far, only theories of the kind LW<sub>112</sub><sup>223</sup> will be used in the remainder of this paper as it has been shown to provide the most accurate results with the least amount of DOF. For the given problem, the chosen theory has 85 DOF, which is magnitudes lower than the number of DOF of the converged FEM model, making the proposed analytical approach computationally efficient. It should be noted, however, that the choice of theory is problem dependent and is influenced by, amongst other factors, the plate's aspect ratio as well

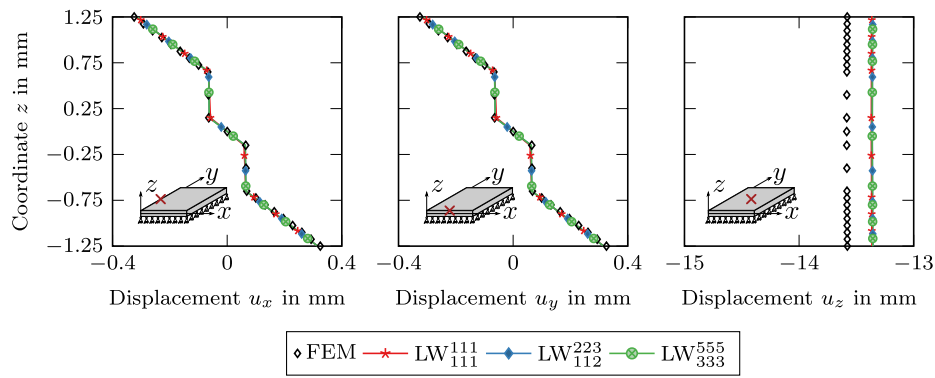


Fig. 5. Through-thickness distribution of displacements for different LW theories.

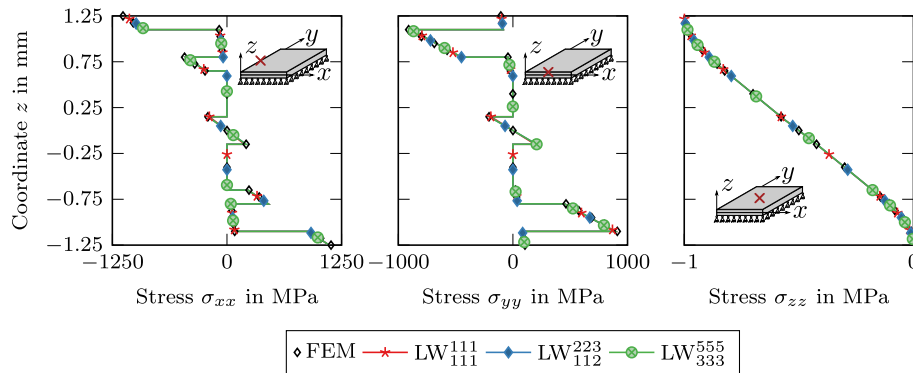


Fig. 6. Through-thickness distribution of normal stresses for different LW theories.

as the quantities, which are to be investigated. This is shown by Petrolo et al. [28] for the RMVT in conjunction with the CUF. For relatively slender plates, the authors also encourage the use of reduced models, as adopted in the present study.

A comparison of the predicted displacement field of theories  $ESL_{112}^{223}$ ,  $Sub_{112}^{223}$  and  $LW_{112}^{223}$  is given in Fig. 7. For the in-plane displacements  $u_x$  and  $u_y$ , the ESL approach differs from the other two as it can be seen as a homogenization across the thickness. While it can globally be seen as a satisfactory approximation, it fails to give insight into the kinematics within the laminate. The displacement component  $u_z$  is greatly underestimated by the ESL approach. The deviation between the other two theories is negligible. For all three displacements, no difference is observed when comparing the sublaminates approach with the full layerwise one. The reason for the underestimation of the transverse displacement  $u_z$  by theory  $ESL_{112}^{223}$  is found by view of the out-of-plane shear strain distribution in Fig. 8. It can be seen that the ESL approach fails to capture the strongly inhomogeneous strain field across the thickness, as only a linear ansatz for the displacement is made for the whole laminate. Noteworthy are the very large transverse shear strains within the elastomer layers, which in turn are the key element of the CLD mechanism investigated in this paper.

The integrated out-of-plane stress components predicted by the three approaches are shown in Fig. 9. It should be noted that even in case of the ESL as well as sublaminates based approaches the out-of-plane stresses are modeled layerwise, as described in Section 3.5. Consequently, the ESL theory yields acceptable results when compared to the sublaminates and layerwise ones, which again are not distinguishable in their predictions for the two out-of-plane shear stresses. No deviations between any of the three theories is observed in case of stress component  $\sigma_{zz}$ . Owing to the results presented so far, the sublaminates based theory  $Sub_{112}^{223}$  is used in the remainder of this work as it yields identical results to the full layerwise theory  $LW_{112}^{223}$  unless local displacement or strain phenomena within the two CFRP sublaminates are of interest. These, however, are not within the scope of this work.

## 5.2. Free vibration

The 25 modes of the simply supported plate under investigation according to Section 4.2 are visualized in Fig. 10. The modes are denoted in terms of their number of half waves ( $m, n$ ) in  $x$ - and  $y$ -direction. It should be noted that the modes considered here do not necessarily correspond to the first 25 modes in order of their occurrence, but are all modes up to five half waves in  $x$ - and  $y$ -direction.

A complete summary of all the natural frequencies and damping ratios is, for reasons of brevity, given in Appendix D Table D.6. It can be summarized, that the undamped natural frequencies  $\bar{f}_{mn}^0$  are almost identical to those determined with FEM, namely  $\bar{f}_{FEM}^0$ . In both cases, the iterative algorithm according to Fig. 4 has not been used as indicated by  $\bar{}$  in the following. The damped natural frequencies, in which the material's viscoelastic behavior is taken into account, are also identical when comparing the proposed analytical approach  $\bar{f}_{mn}$  without iteration and the FEM solution  $\bar{f}_{FEM}$  and lie in proximity to the undamped ones. The corresponding modal damping ratios  $\bar{\xi}_{mn}$  and  $\bar{\xi}_{FEM}$  are also almost identical, verifying the proposed analytical model for undamped and damped natural frequencies. In both cases, the frequency-dependent stiffness of the elastomer material has been evaluated according to its long-term behavior at the lowest frequency in Fig. 1. However, as there is an increase in the shear modulus, a stiffer material behavior is expected when excited at higher frequencies. This is confirmed by the iterated undamped natural frequencies  $f_{mn}^0$  in Table D.6 which have been determined by using the algorithm outlined in Fig. 4 in Section 3.6.2. This is also observed in the case of the damped natural frequencies in Table D.6 and Fig. 11, which shows a comparison of damped natural frequencies determined non-iteratively using FEM  $\bar{f}_{FEM}$ , non-iteratively with the analytical model  $\bar{f}_{mn}$  and iteratively with the analytical model, namely  $f_{mn}$ . The modes calculated iteratively occur at significantly higher frequencies. The deviation increases for the higher modes, which can be explained by the increase of the shear

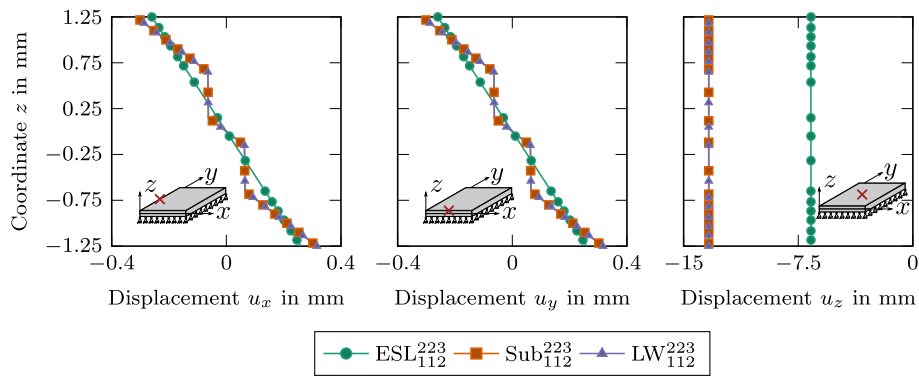


Fig. 7. Through-thickness distribution of displacement components for an equivalent-single-layer, layerwise and sublaminated based theory.

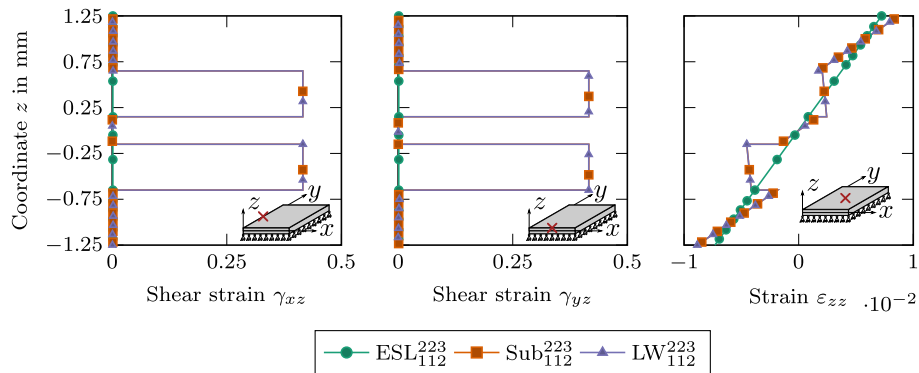


Fig. 8. Through-thickness distribution of out-of-plane strain components for an equivalent-single-layer, layerwise and sublaminated based theory.

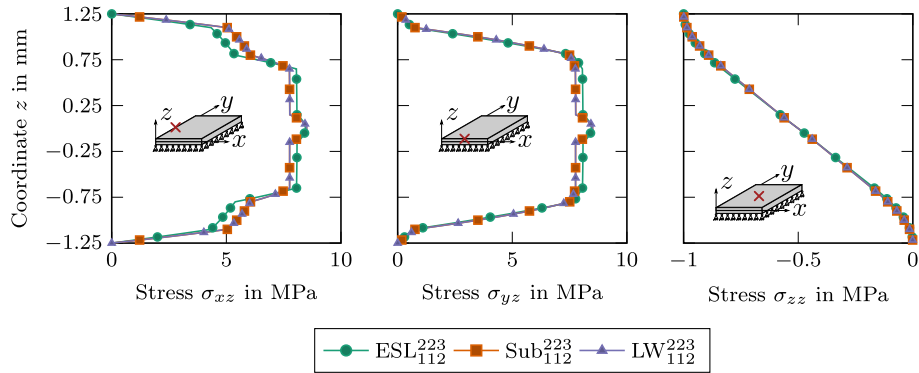


Fig. 9. Through-thickness distribution of out-of-plane stress components for an equivalent-single-layer, layerwise and sublaminated based theory.

modulus in Fig. 1 in the frequency spectrum of interest  $\omega = 1 \times 10^{-1} \text{ s}^{-1}$  to  $1 \times 10^3 \text{ s}^{-1}$ . When comparing the modal damping ratios  $\hat{\xi}_{\text{FEM}}$ ,  $\hat{\xi}_{mn}$  and  $\xi_{mn}$  in Fig. 12, the aforementioned agreement of the proposed analytical approach with the FEM solution clearly shows. Generally, it can be observed that higher modes also tend to show a higher modal damping. The reason for the increase in modal damping with higher modes is found in the state of deformation when more half-waves are present in the plate. These lead to higher transverse shear strains in the elastomer layers and thus to more dissipation due to the material's viscoelastic properties. A similar aspect is visible when comparing corresponding modes such as (1, 2) and (2, 1). In this case, stronger damping occurs in the mode with more half waves in  $y$ -direction than in  $x$ -direction. In this case, the elastomer damping layers can deform more in  $y$ -direction than in  $x$ -direction due to the lower overall laminate stiffness of the laminate in  $y$ -direction attributed to the given laminate layup and fiber orientations. The modal damping ratios calculated with the iterative algorithm  $\xi_{mn}$ , however, are significantly lower while still showing an

increase with higher modes due to the aforementioned correlation. The increase is less pronounced than that observed in the damping ratios not calculated iteratively. This is due to the decrease in the elastomer material's loss factor  $\tan(\delta)$  as shown in Fig. 1 which is now taken into account. The relative difference between results obtained non-iteratively and iteratively is significantly higher in case of the modal damping ratios than it is for the undamped and damped natural frequencies.

A variation of the elastomer's complex shear modulus with the scaling factor  $\kappa$  leads to the results shown in Fig. 13 for the first ten modes. Generally, an increase in stiffness leads to higher natural frequencies for a given mode. Higher modes show a larger relative shift than lower ones. Conversely, when looking at the change in modal damping ratio, lower modes are influenced to a larger extent by a varying stiffness than the higher modes. It can also be stated that the influence of varying stiffness is lower on the natural frequency than on the modal damping ratio for all modes shown here.

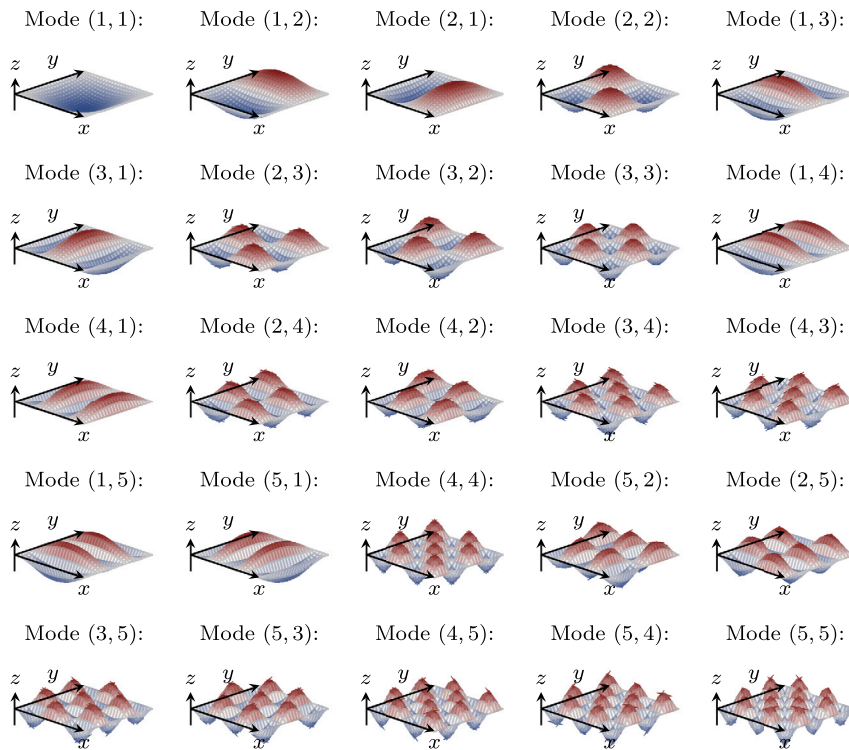


Fig. 10. Visualization of 25 mode shapes occurring in the simply supported HyCEML plate in terms of the normalized displacement  $\tilde{u}_n$ .

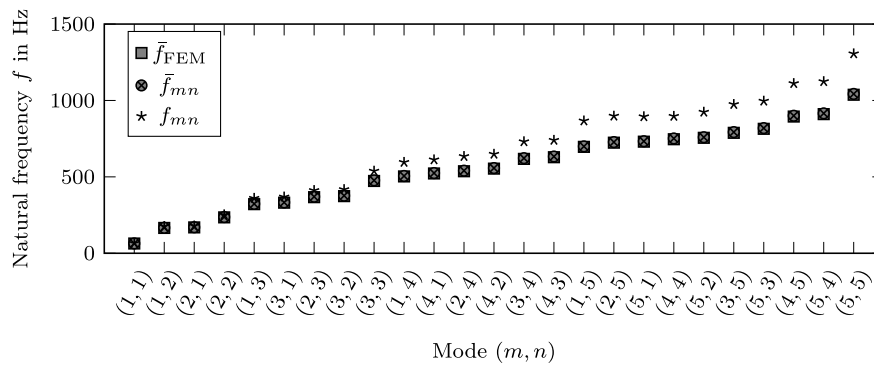


Fig. 11. Damped natural frequencies determined non-iteratively using FEM,  $\tilde{f}_{FEM}$ , as well as non-iteratively and iteratively,  $\tilde{f}_{mn}$  and  $f_{mn}$ , using the proposed analytical model.

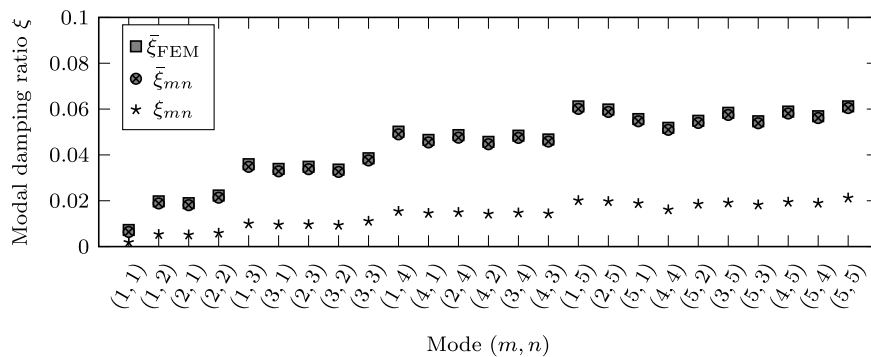


Fig. 12. Modal damping ratios determined non-iteratively using FEM,  $\tilde{\xi}_{FEM}$ , as well as non-iteratively and iteratively,  $\tilde{\xi}_{mn}$  and  $\xi_{mn}$ , using the proposed analytical model.

Fig. 14 displays the influence of a variation of the elastomer layers' thickness on the natural frequencies and modal damping ratios for the same ten modes. A higher thickness leads to higher natural frequencies as the overall laminate stiffness is increased. This is particularly true for

lower modes compared to higher ones. A similar effect is observed for the modal damping ratios which are also increased by higher elastomer layer thicknesses. Again, this effect is more pronounced for lower modes than for higher ones. Generally, the effect of the elastomer layer

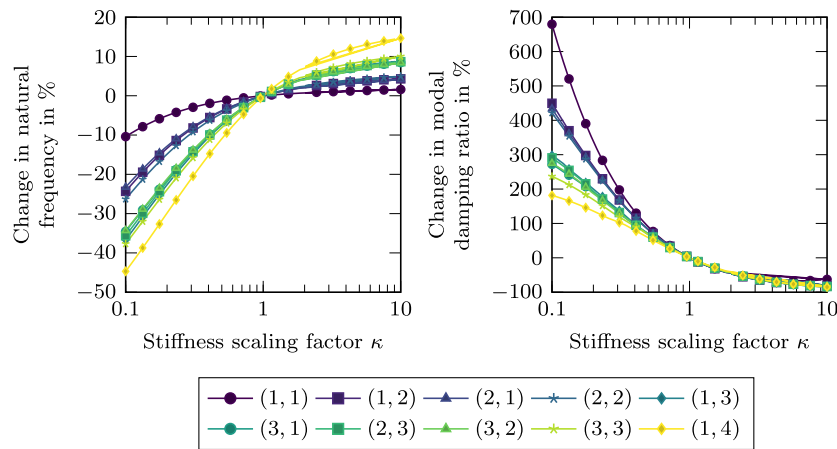


Fig. 13. Influence of scaled elastomer stiffness on the natural frequency and modal damping factor. Increasing brightness represents higher modes.

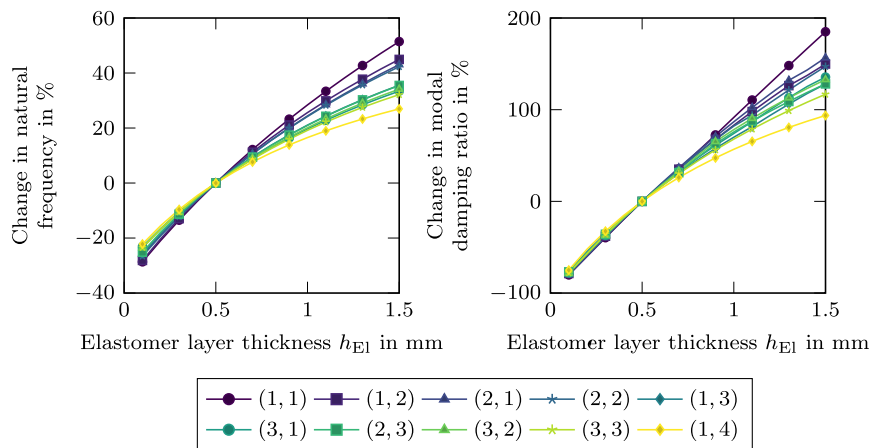


Fig. 14. Influence of elastomer layer thickness on the natural frequency and modal damping factor. A thickness of  $t = 0.50\text{mm}$  is taken as reference, as it corresponds to the laminate considered in the remainder of the paper. Increasing brightness represents higher modes.

thickness on the modal damping ratio is higher than on the natural frequency.

### 5.3. Forced vibration

The response of the HyCEML plate to a forced vibration is shown in Fig. 15 in terms of displacement amplitude  $\|\hat{u}_z^*\|$  and Fig. 16 for the corresponding phase angle  $\delta$ . For comparison, the natural frequencies  $f_{mn}$  from Table D.6 are also included as vertical lines. It can be noted that the frequency response differs depending on the point at which the plate is excited. An excitation in the center of the plate, namely Point C in Fig. 3, generally leads to higher displacement amplitudes, but fewer modes are excited, which are identified as peaks in amplitude coinciding with the natural frequencies. An excitation in Point D leads to lower amplitudes while exciting more modes. In case of an excitation in Point E, every mode is excited and distinguishable in the frequency response. When taking the width of each peak as a measure for the modal damping, the previously observed trend of higher modal damping with higher modes can also be observed in the frequency response shown in Fig. 15.

Fig. 16 shows the phase angle between force excitation and the plate's response in terms of transverse displacement. Again, the natural frequencies from Table D.6 are shown for comparison. Excited modes can be identified by a shift in the phase angle  $\delta$  of  $\pi$  or less, depending on the damping of the mode. Consequently, higher modal damping factors lead to smaller shift in phase angle. For higher excitation

frequencies, the distinct modes become harder to identify based on the phase angle in Fig. 16 alone.

The forced vibration analysis shows exact agreement with the natural frequencies determined using the iterative algorithm outlined in Fig. 4. This highlights the importance of iterative procedures when calculating the natural frequencies and modal damping ratios of laminates containing frequency-dependent materials such as the elastomer in this study. Consequently, common approaches not accounting for frequency-dependent material behavior do not suffice when the dynamic behavior of constrained layer damping laminates is to be analyzed. Iterative algorithms such as the one presented here or in [56] are thus preferable.

## 6. Conclusions

This study introduces an analytical modeling approach based on the Generalized Unified Formulation (GUF) for hybrid laminates containing elastomer layers in order to realize intrinsic damping, the so called constrained layer damping (CLD). The developed approach for simply supported plates adopts a sublaminates based assembly procedure, coupling layerwise and equivalent single layer (ESL) theories. This analytical modeling approach, requiring a minimum amount of DOF, allows for an accurate analysis of the static and dynamic behavior of laminates, as shown in Section 5, containing viscoelastic damping layers present in CLD applications. The novelties of this paper include the application of the Reissner's Mixed Variational Theorem (RMVT) using a sublaminates GUF for the dynamic analysis of viscoelastic laminates.

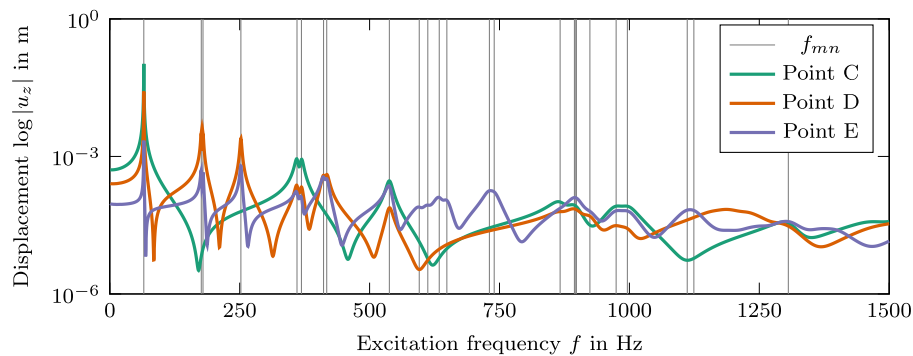


Fig. 15. Frequency response in terms of displacement amplitude  $\|u_z\|$  over excitation frequency  $f$  for three different excitation points. For comparison, the natural frequencies  $f_{mn}$  are also shown.

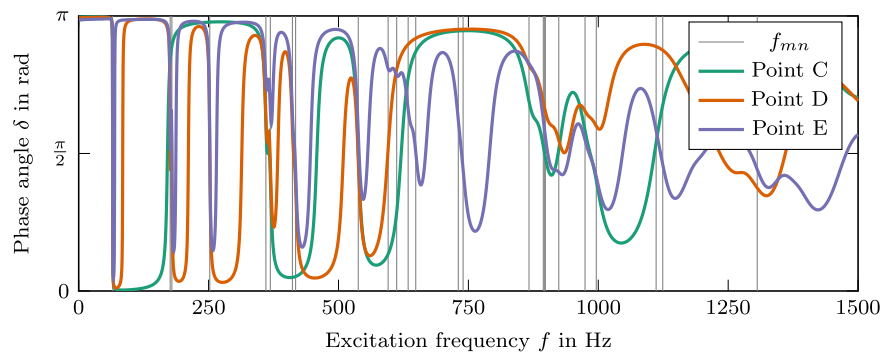


Fig. 16. Frequency response in terms of phase angle  $\delta$  over excitation frequency  $f$  for three different excitation points  $C$ ,  $D$  and  $E$  corresponding to Fig. 3. For comparison, the natural frequencies  $f_{mn}$  are also shown.

By comparison with refined FEM models, this sublaminar approach is found to be highly accurate and yield identical results as the full layerwise theories whilst featuring significantly less degrees of freedom (DOF), making it the approach of choice for the analysis of hybrid laminates by judgment of the authors.

Free vibration analysis using an iterative algorithm in order to account for the elastomer's frequency-dependent mechanical behavior is conducted. The natural frequencies and modal damping ratios are determined and compared to FEM solutions. A significant shift in the calculated natural frequencies is observed when the iterative algorithm is used. The modal damping ratios in this paper are shown to be influenced even more by the use of an iterative algorithm. As these results agree well with the peaks seen in the frequency response of the plate to forced vibration, it can be concluded that the frequency-dependent stiffness of the damping material should be considered, for example by adopting the iterative algorithm introduced here. This applies, in particular, when accurate predictions on the dynamic behavior of CLD laminates are to be made.

Furthermore, the free vibration analysis has shown that the properties of the elastomer damping layers significantly influence how the laminate is damped. While a decrease in stiffness of the elastomer layer leads to slightly lower natural frequencies, the modal damping is increased significantly, especially for lower modes. An increase in the elastomer layer thickness on the other hand leads to higher natural frequencies, but also increases the modal damping ratio. Again, the effect is more pronounced for lower modes. It is concluded that the choice of laminate and damping material allow for the specific design of lightweight laminates regarding its desired damping behavior.

From a theoretical point of view, the analytical modeling approach based on the GUF presented here could be extended to consider material nonlinearities, especially those of the elastomer material, in order to analyze possible nonlinear effects in the plate's frequency response. Future works could also include the practical application of the CLD

modeling approach to optimize the lamination scheme for maximum damping. The use of machine learning algorithms could also be considered in order to find optimal parameter sets regarding material properties, lamination scheme and plate dimensions in order to achieve maximum intrinsic damping with admissible compliance at the lowest weight possible.

#### CRediT authorship contribution statement

**Alexander Jackstadt:** Conceptualization, Methodology, Software, Investigation, Writing – original draft. **Wilfried V. Liebig:** Conceptualization, Writing – review & editing. **Luise Kärger:** Supervision, Writing – review & editing.

#### Declaration of competing interest

The authors declare that they have no known competing financial interests or personal relationships that could have appeared to influence the work reported in this paper.

#### Acknowledgments

This work is funded by the Deutsche Forschungsgemeinschaft (DFG, German Research Foundation) SPP1897 “Calm, Smooth, Smart — Novel approaches for influencing vibrations by means of deliberately introduced dissipation”, project KA 4224/3-2 “HyCEML — Hybrid CFRP/elastomer/metal laminates containing elastomeric interfaces for deliberate dissipation” (Karlsruhe Institute of Technology). The work is also part of the Young Investigator Group (YIG) “Green Mobility”, generously funded by the Vector Stiftung, Germany. Furthermore, the authors would like to acknowledge Gummiwerk KRAIBURG GmbH & Co. KG for providing the elastomer material. Special gratitude is given to Vincent Sessner who provided the experimental data used for material modeling.

## Appendix A. Constitutive relation

The orthotropic linear elastic behavior in this paper is represented by the following classic form of Hooke's law

$$\begin{Bmatrix} \sigma_p \\ \sigma_n \end{Bmatrix} = \begin{Bmatrix} \hat{C}_{pp} & \hat{C}_{pn} \\ \hat{C}_{np} & \hat{C}_{nn} \end{Bmatrix} \begin{Bmatrix} \varepsilon_p \\ \varepsilon_n \end{Bmatrix} \quad (\text{A.1})$$

in a modified Voigt notation

$$\begin{bmatrix} \sigma_{11} \\ \sigma_{22} \\ \sigma_{12} \\ \sigma_{13} \\ \sigma_{23} \\ \sigma_{33} \end{bmatrix} = \begin{bmatrix} \hat{C}_{11} & \hat{C}_{12} & \hat{C}_{14} & 0 & 0 & \hat{C}_{13} \\ \hat{C}_{12} & \hat{C}_{22} & \hat{C}_{24} & 0 & 0 & \hat{C}_{23} \\ \hat{C}_{14} & \hat{C}_{24} & \hat{C}_{44} & 0 & 0 & \hat{C}_{34} \\ 0 & 0 & 0 & \hat{C}_{55} & \hat{C}_{56} & 0 \\ 0 & 0 & 0 & \hat{C}_{56} & \hat{C}_{66} & 0 \\ \hat{C}_{13} & \hat{C}_{23} & \hat{C}_{34} & 0 & 0 & \hat{C}_{33} \end{bmatrix} \begin{bmatrix} \varepsilon_{11} \\ \varepsilon_{22} \\ \gamma_{12} \\ \gamma_{13} \\ \gamma_{23} \\ \varepsilon_{33} \end{bmatrix} \quad (\text{A.2})$$

with  $\sigma_p = [\sigma_{11} \ \sigma_{22} \ \sigma_{12}]^T$  and  $\sigma_n = [\sigma_{13} \ \sigma_{23} \ \sigma_{33}]^T$ . Strains  $\varepsilon_p$  and  $\varepsilon_n$  are defined accordingly. The components of the stiffness matrix  $C$  from Eq. (A.4) can be calculated by the following relations:

$$\begin{aligned} C_{pp} &= \hat{C}_{pp} - \hat{C}_{pn} \hat{C}_{nn}^{-1} \hat{C}_{np} \\ C_{pn} &= \hat{C}_{pn} \hat{C}_{nn}^{-1} \\ C_{np} &= -\hat{C}_{nn}^{-1} \hat{C}_{np} \\ C_{nn} &= \hat{C}_{nn}^{-1}. \end{aligned} \quad (\text{A.3})$$

Following the transformations in Eq. (A.3) the mixed form of Hooke's law is given by

$$\begin{bmatrix} \sigma_{11} \\ \sigma_{22} \\ \sigma_{12} \\ \gamma_{13} \\ \gamma_{23} \\ \sigma_{33} \end{bmatrix} = \begin{bmatrix} C_{11} & C_{12} & C_{14} & 0 & 0 & C_{13} \\ C_{12} & C_{22} & C_{24} & 0 & 0 & C_{23} \\ C_{14} & C_{24} & C_{44} & 0 & 0 & C_{34} \\ 0 & 0 & 0 & C_{55} & C_{56} & 0 \\ 0 & 0 & 0 & C_{56} & C_{66} & 0 \\ -C_{13} & -C_{23} & -C_{34} & 0 & 0 & C_{33} \end{bmatrix} \begin{bmatrix} \varepsilon_{11} \\ \varepsilon_{22} \\ \gamma_{12} \\ \sigma_{13} \\ \sigma_{23} \\ \sigma_{33} \end{bmatrix} \quad (\text{A.4})$$

and is used in the formulation of kernel matrices.

## Appendix B. Governing equations

The following variational equations with regard to displacements and out-of-plane stresses result from Eq. (4):

$$\begin{aligned} \delta u_{x\alpha_x} : & -C_{11}^k \frac{\partial^2 \Phi_x}{\partial x^2} \int_{z_{\text{bot}}^k}^{z_{\text{top}}^k} F_{\alpha_x} F_{\beta_x} dz U_{x\beta_x}^k \\ & -C_{12}^k \frac{\partial^2 \Phi_y}{\partial x \partial y} \int_{z_{\text{bot}}^k}^{z_{\text{top}}^k} F_{\alpha_x} F_{\beta_y} dz U_{y\beta_y}^k \\ & -C_{13}^k \frac{\partial \Phi_z}{\partial x} \int_{z_{\text{bot}}^k}^{z_{\text{top}}^k} F_{\alpha_x} F_{\beta_{zz}} dz S_{zz\beta_{zz}}^k \\ & -C_{44}^k \frac{\partial^2 \Phi_x}{\partial y^2} \int_{z_{\text{bot}}^k}^{z_{\text{top}}^k} F_{\alpha_x} F_{\beta_x} dz U_{x\beta_x}^k \\ & -C_{44}^k \frac{\partial^2 \Phi_y}{\partial x \partial y} \int_{z_{\text{bot}}^k}^{z_{\text{top}}^k} F_{\alpha_x} F_{\beta_y} dz U_{y\beta_y}^k \\ & + \Phi_x \int_{z_{\text{bot}}^k}^{z_{\text{top}}^k} \frac{dF_{\alpha_x}}{dz} F_{\beta_{xz}} dz S_{xz\beta_{xz}}^k \\ & + \rho^k \Phi_x \int_{z_{\text{bot}}^k}^{z_{\text{top}}^k} F_{\alpha_x} F_{\beta_x} dz \ddot{U}_{x\beta_x}^k \\ & = \Phi_x F_{\alpha_x} |_{z=z_{\text{top}}^k} Q_x^{k,\text{top}} + \Phi_x F_{\alpha_x} |_{z=z_{\text{bot}}^k} Q_x^{k,\text{bot}} \end{aligned} \quad (\text{B.1})$$

$$\begin{aligned} \delta u_{y\alpha_y} : & -C_{12}^k \frac{\partial^2 \Phi_x}{\partial x \partial y} \int_{z_{\text{bot}}^k}^{z_{\text{top}}^k} F_{\alpha_y} F_{\beta_x} dz U_{x\beta_x}^k \\ & -C_{22}^k \frac{\partial^2 \Phi_y}{\partial y^2} \int_{z_{\text{bot}}^k}^{z_{\text{top}}^k} F_{\alpha_y} F_{\beta_y} dz U_{y\beta_y}^k \\ & -C_{23}^k \frac{\partial \Phi_z}{\partial y} \int_{z_{\text{bot}}^k}^{z_{\text{top}}^k} F_{\alpha_y} F_{\beta_{zz}} dz S_{zz\beta_{zz}}^k \\ & -C_{44}^k \frac{\partial^2 \Phi_x}{\partial x \partial y} \int_{z_{\text{bot}}^k}^{z_{\text{top}}^k} F_{\alpha_y} F_{\beta_x} dz U_{x\beta_x}^k \\ & -C_{44}^k \frac{\partial^2 \Phi_y}{\partial x^2} \int_{z_{\text{bot}}^k}^{z_{\text{top}}^k} F_{\alpha_y} F_{\beta_y} dz U_{y\beta_y}^k \\ & + \Phi_y \int_{z_{\text{bot}}^k}^{z_{\text{top}}^k} \frac{dF_{\alpha_y}}{dz} F_{\beta_{yz}} dz S_{yz\beta_{yz}}^k \\ & + \rho^k \Phi_y \int_{z_{\text{bot}}^k}^{z_{\text{top}}^k} F_{\alpha_y} F_{\beta_y} dz \ddot{U}_{y\beta_y}^k \\ & = \Phi_y F_{\alpha_y} |_{z=z_{\text{top}}^k} Q_y^{k,\text{top}} + \Phi_y F_{\alpha_y} |_{z=z_{\text{bot}}^k} Q_y^{k,\text{bot}} \end{aligned} \quad (\text{B.2})$$

$$\begin{aligned} \delta u_{z\alpha_z} : & -\frac{\partial \Phi_x}{\partial x} \int_{z_{\text{bot}}^k}^{z_{\text{top}}^k} F_{\alpha_z} F_{\beta_{xz}} dz S_{xz\beta_{xz}}^k \\ & -\frac{\partial \Phi_y}{\partial y} \int_{z_{\text{bot}}^k}^{z_{\text{top}}^k} F_{\alpha_z} F_{\beta_{yz}} dz S_{yz\beta_{yz}}^k \\ & + \Phi_z \int_{z_{\text{bot}}^k}^{z_{\text{top}}^k} \frac{dF_{\alpha_z}}{dz} F_{\beta_{zz}} dz S_{zz\beta_{zz}}^k \\ & + \rho^k \Phi_z \int_{z_{\text{bot}}^k}^{z_{\text{top}}^k} F_{\alpha_z} F_{\beta_z} dz \ddot{U}_{z\beta_z}^k \\ & = \Phi_z F_{\alpha_z} |_{z=z_{\text{top}}^k} Q_z^{k,\text{top}} + \Phi_z F_{\alpha_z} |_{z=z_{\text{bot}}^k} Q_z^{k,\text{bot}} \end{aligned} \quad (\text{B.3})$$

$$\begin{aligned} \delta \sigma_{xz\alpha_{xz}} : & \Phi_x \int_{z_{\text{bot}}^k}^{z_{\text{top}}^k} F_{\alpha_{xz}} \frac{dF_{\beta_x}}{dz} U_{x\beta_x}^k \\ & + \frac{\partial \Phi_z}{\partial x} \int_{z_{\text{bot}}^k}^{z_{\text{top}}^k} F_{\alpha_{xz}} F_{\beta_z} dz U_{z\beta_z}^k \\ & - C_{55} \int_{z_{\text{bot}}^k}^{z_{\text{top}}^k} F_{\alpha_{xz}} F_{\beta_{xz}} dz S_{xz\beta_{xz}}^k \\ & = 0 \end{aligned} \quad (\text{B.4})$$

$$\begin{aligned} \delta \sigma_{yz\alpha_{yz}} : & \Phi_y \int_{z_{\text{bot}}^k}^{z_{\text{top}}^k} F_{\alpha_{yz}} \frac{dF_{\beta_y}}{dz} U_{y\beta_y}^k \\ & + \frac{\partial \Phi_z}{\partial y} \int_{z_{\text{bot}}^k}^{z_{\text{top}}^k} F_{\alpha_{yz}} F_{\beta_z} dz U_{z\beta_z}^k \\ & - C_{66} \int_{z_{\text{bot}}^k}^{z_{\text{top}}^k} F_{\alpha_{yz}} F_{\beta_{yz}} dz S_{yz\beta_{yz}}^k \\ & = 0 \end{aligned} \quad (\text{B.5})$$

$$\begin{aligned} \delta \sigma_{zz\alpha_{zz}} : & \Phi_z \int_{z_{\text{bot}}^k}^{z_{\text{top}}^k} F_{\alpha_{zz}} \frac{dF_{\beta_z}}{dz} U_{z\beta_z}^k \\ & + C_{13}^k \frac{\partial \Phi_x}{\partial x} \int_{z_{\text{bot}}^k}^{z_{\text{top}}^k} F_{\alpha_{zz}} F_{\beta_x} dz U_{x\beta_x}^k \\ & + C_{23}^k \frac{\partial \Phi_y}{\partial y} \int_{z_{\text{bot}}^k}^{z_{\text{top}}^k} F_{\alpha_{zz}} F_{\beta_y} dz U_{y\beta_y}^k \\ & - C_{33}^k \Phi_z \int_{z_{\text{bot}}^k}^{z_{\text{top}}^k} F_{\alpha_{zz}} F_{\beta_{zz}} dz S_{zz\beta_{zz}}^k \\ & = 0 \end{aligned} \quad (\text{B.6})$$

**Table D.6**

Undamped and damped natural frequencies  $f$  and damping ratios  $\xi$  corresponding to the modes of a simply supported HyCEML plate in Fig. 10.

Mode	$f_{FEM}^0$ in Hz	$f_{mn}^0$ in Hz	$f_{mn}^0$ in Hz	$\bar{f}_{FEM}$ in Hz	$\bar{\xi}_{FEM}$	$\bar{f}_{mn}$ in Hz	$f_{mn}$ in Hz	$\bar{\xi}_{mn}$	$\xi_{mn}$
(1, 1)	63.78	64.27	65.40	63.78	0.0290	64.32	0.0064	65.42	0.0019
(1, 2)	165.70	166.62	176.01	165.73	0.0790	166.84	0.0188	176.07	0.0053
(2, 1)	169.19	170.09	179.30	169.22	0.0758	170.31	0.0181	179.36	0.0051
(2, 2)	234.86	236.71	252.18	234.91	0.0892	237.05	0.0213	252.28	0.0059
(1, 3)	321.14	322.92	360.13	321.35	0.1438	323.32	0.0348	360.28	0.0100
(3, 1)	330.72	332.41	368.68	330.91	0.1356	332.80	0.0328	368.82	0.0095
(2, 3)	366.87	369.68	411.17	367.09	0.1394	370.15	0.0338	411.36	0.0096
(3, 2)	373.72	376.45	417.27	373.93	0.1344	376.91	0.0326	417.46	0.0093
(3, 3)	472.76	476.58	537.78	473.11	0.1542	477.10	0.0376	538.05	0.0111
(1, 4)	502.29	505.51	595.31	502.92	0.2006	505.64	0.0490	595.56	0.0154
(4, 1)	521.69	524.71	611.74	522.25	0.1862	524.84	0.0455	612.00	0.0145
(2, 4)	536.16	540.32	633.77	536.80	0.1946	540.49	0.0475	634.06	0.0149
(4, 2)	553.31	557.27	648.39	553.89	0.1828	557.45	0.0447	648.68	0.0142
(3, 4)	616.96	622.08	730.23	617.68	0.1936	622.29	0.0474	730.58	0.0147
(4, 3)	627.90	632.89	739.47	628.58	0.1870	633.09	0.0458	739.82	0.0143
(1, 5)	695.07	700.15	866.41	696.38	0.2447	699.37	0.0601	866.68	0.0201
(2, 5)	722.40	728.30	893.94	723.69	0.2393	727.56	0.0588	894.22	0.0188
(5, 1)	729.13	733.85	896.46	730.26	0.2226	733.11	0.0547	896.88	0.0161
(4, 4)	745.28	751.46	897.70	746.29	0.2073	751.38	0.0509	898.01	0.0197
(5, 2)	754.44	759.98	923.67	755.58	0.2196	759.27	0.0539	923.98	0.0185
(3, 5)	786.81	793.57	974.13	788.16	0.2336	792.86	0.0574	974.49	0.0191
(5, 3)	813.22	819.66	995.75	814.43	0.2188	818.98	0.0538	996.13	0.0182
(4, 5)	893.15	900.81	1110.90	894.70	0.2357	899.88	0.0581	1111.33	0.0194
(5, 4)	909.03	916.51	1123.64	910.51	0.2276	915.60	0.0561	1124.07	0.0190
(5, 5)	1035.50	1044.26	1305.46	1037.40	0.2448	1042.64	0.0604	1305.91	0.0212

**Appendix C. Kernel matrices**

The following kernel matrices are derived from Appendix B and used in the formulation of the global system of equations in Eq. (12).

Stiffness kernel matrices:

$$\mathbf{K}_{U_x U_x}^k \hat{=} \frac{1}{\Phi_x} \left( -C_{11}^k \frac{\partial^2 \Phi_x}{\partial x^2} \int_{z_{bot}^k}^{z_{top}^k} F_{\alpha_x} F_{\beta_x} dz - C_{44}^k \frac{\partial^2 \Phi_x}{\partial y^2} \int_{z_{bot}^k}^{z_{top}^k} F_{\alpha_x} F_{\beta_x} dz \right) \tag{C.1}$$

$$\mathbf{K}_{U_x U_y}^k \hat{=} \frac{1}{\Phi_x} \left( -C_{12}^k \frac{\partial^2 \Phi_y}{\partial x \partial y} \int_{z_{bot}^k}^{z_{top}^k} F_{\alpha_x} F_{\beta_y} dz - C_{44}^k \frac{\partial^2 \Phi_y}{\partial x \partial y} \int_{z_{bot}^k}^{z_{top}^k} F_{\alpha_x} F_{\beta_y} dz \right) \tag{C.2}$$

$$\mathbf{K}_{U_x S_x}^k \hat{=} \int_{z_{bot}^k}^{z_{top}^k} \frac{dF_{\alpha_x}}{dz} F_{\beta_{xz}} dz \tag{C.3}$$

$$\mathbf{K}_{U_x S_z}^k \hat{=} \frac{1}{\Phi_x} \left( -C_{13}^k \frac{\partial \Phi_z}{\partial x} \int_{z_{bot}^k}^{z_{top}^k} F_{\alpha_x} F_{\beta_{zz}} dz \right) \tag{C.4}$$

$$\mathbf{K}_{U_y U_y}^k \hat{=} \frac{1}{\Phi_y} \left( -C_{22}^k \frac{\partial^2 \Phi_y}{\partial y^2} \int_{z_{bot}^k}^{z_{top}^k} F_{\alpha_y} F_{\beta_y} dz - C_{44}^k \frac{\partial^2 \Phi_y}{\partial x^2} \int_{z_{bot}^k}^{z_{top}^k} F_{\alpha_y} F_{\beta_y} dz \right) \tag{C.5}$$

$$\mathbf{K}_{U_y S_y}^k \hat{=} \int_{z_{bot}^k}^{z_{top}^k} \frac{dF_{\alpha_y}}{dz} F_{\beta_{yz}} dz \tag{C.6}$$

$$\mathbf{K}_{U_y S_z}^k \hat{=} \frac{1}{\Phi_y} \left( -C_{23}^k \frac{\partial \Phi_z}{\partial y} \int_{z_{bot}^k}^{z_{top}^k} F_{\alpha_y} F_{\beta_{zz}} dz \right) \tag{C.7}$$

$$\mathbf{K}_{U_z S_x}^k \hat{=} \frac{1}{\Phi_x} \left( -\frac{\partial \Phi_x}{\partial x} \int_{z_{bot}^k}^{z_{top}^k} F_{\alpha_z} F_{\beta_{xz}} dz \right) \tag{C.8}$$

$$\mathbf{K}_{U_z S_y}^k \hat{=} \frac{1}{\Phi_y} \left( -\frac{\partial \Phi_y}{\partial y} \int_{z_{bot}^k}^{z_{top}^k} F_{\alpha_z} F_{\beta_{yz}} dz \right) \tag{C.9}$$

$$\mathbf{K}_{U_z S_z}^k \hat{=} \int_{z_{bot}^k}^{z_{top}^k} \frac{dF_{\alpha_z}}{dz} F_{\beta_{zz}} dz \tag{C.10}$$

$$\mathbf{K}_{S_x S_x}^k \hat{=} -C_{55} \int_{z_{bot}^k}^{z_{top}^k} F_{\alpha_{xz}} F_{\beta_{xz}} dz \tag{C.11}$$

$$\mathbf{K}_{S_y S_y}^k \hat{=} -C_{66} \int_{z_{bot}^k}^{z_{top}^k} F_{\alpha_{yz}} F_{\beta_{yz}} dz \tag{C.12}$$

$$\mathbf{K}_{S_z S_z}^k \hat{=} -C_{33}^k \Phi_z \int_{z_{bot}^k}^{z_{top}^k} F_{\alpha_{zz}} F_{\beta_{zz}} dz \tag{C.13}$$

Mass kernel matrices:

$$\mathbf{M}_{U_x U_x}^k \hat{=} \rho^k \int_{z_{bot}^k}^{z_{top}^k} F_{\alpha_x} F_{\beta_x} dz \tag{C.14}$$

$$\mathbf{M}_{U_y U_y}^k \hat{=} \rho^k \int_{z_{bot}^k}^{z_{top}^k} F_{\alpha_y} F_{\beta_y} dz \tag{C.15}$$

$$\mathbf{M}_{U_z U_z}^k \hat{=} \rho^k \int_{z_{bot}^k}^{z_{top}^k} F_{\alpha_z} F_{\beta_z} dz \tag{C.16}$$

Load kernel vectors:

$$\mathbf{R}_x^k \hat{=} F_{\alpha_x} |_{z=z_{top}^k} Q_x^{k,top} + F_{\alpha_x} |_{z=z_{bot}^k} Q_x^{k,bot} \tag{C.17}$$

$$\mathbf{R}_y^k \hat{=} F_{\alpha_y} |_{z=z_{top}^k} Q_y^{k,top} + F_{\alpha_y} |_{z=z_{bot}^k} Q_y^{k,bot} \tag{C.18}$$

$$\mathbf{R}_z^k \hat{=} F_{\alpha_z} |_{z=z_{top}^k} Q_z^{k,top} + F_{\alpha_z} |_{z=z_{bot}^k} Q_z^{k,bot} \tag{C.19}$$

**Appendix D. Natural frequencies and modal damping ratios**

Table D.6 shows the natural frequencies and modal damping ratios corresponding to the studies outlined in Section 4.2. Undamped frequencies are denoted by  $f^0$ . Modal damping ratios are named  $\xi$ . Quantities which are calculated based on the proposed analytical model are indexed as  $(\ )_{mn}$ . The index  $(\ )_{FEM}$  consequently denotes quantities calculated using the FEM. When the proposed iterative algorithm is not used, the result is marked by  $(\ )_{\bar{\cdot}}$ .

**References**

- [1] Alderliesten R. Fatigue and fracture of fibre metal laminates. Solid mechanics and its applications, vol. 236, Cham: Springer International Publishing; 2017, <http://dx.doi.org/10.1007/978-3-319-56227-8>.
- [2] Oberst H, Frankenfeld K. Über die dämpfung der biegeschwingungen dünner bleche durch fest haftende beläge. Acta Acust United with Acust 1952;2(Supplement 4):181-94.

- [3] Kerwin EM. Damping of flexural waves by a constrained viscoelastic layer. *J Acoust Soc Am* 1959;31(7):952–62. <http://dx.doi.org/10.1121/1.1907821>.
- [4] Rao MD. Recent applications of viscoelastic damping for noise control in automobiles and commercial airplanes. *J Sound Vib* 2003;262(3):457–74. [http://dx.doi.org/10.1016/S0022-460X\(03\)00106-8](http://dx.doi.org/10.1016/S0022-460X(03)00106-8).
- [5] Zhou XQ, Yu DY, Shao XY, Zhang SQ, Wang S. Research and applications of viscoelastic vibration damping materials: A review. *Compos Struct* 2016;136:460–80. <http://dx.doi.org/10.1016/j.compstruct.2015.10.014>.
- [6] Stoll M, Stemmer F, Ilinzeer S, Weidenmann KA. Optimization of corrosive properties of carbon fiber reinforced aluminum laminates due to integration of an elastomer interlayer. *Key Eng Mater* 2017;742 KEM:287–93. <http://dx.doi.org/10.4028/www.scientific.net/KEM.742.287>.
- [7] Liebig WV, Sessner V, Weidenmann KA, Kärger L. Numerical and experimental investigations of the damping behaviour of hybrid CFRP-elastomer-metal laminates. *Compos Struct* 2018;202:1109–13. <http://dx.doi.org/10.1016/j.compstruct.2018.05.051>.
- [8] Sessner V, Liebig WV, Kärger L, Weidenmann KA. Experimental and numerical characterisation of fibre-metal-elastomer laminates by using DMA regarding its damping behaviour. *Pamm* 2018;18(1):e201800432. <http://dx.doi.org/10.1002/pamm.201800432>.
- [9] Sessner V, Jackstadt A, Liebig WV, Kärger L, Weidenmann KA. Damping characterization of hybrid carbon fiber elastomer metal laminates using experimental and numerical dynamic mechanical analysis. *J Compos Sci* 2019;3(1):3. <http://dx.doi.org/10.3390/jcs3010003>.
- [10] Sessner V, Liebig WV, Weidenmann KA. Modal damping behavior of plane and 3D curved constrained layer damping CFRP-elastomer-metal laminates. *Compos Part C Open Access* 2020;2(September):100037. <http://dx.doi.org/10.1016/j.jcomc.2020.100037>.
- [11] Sarlin E, Liu Y, Vippola M, Zogg M, Ermanni P, Vuorinen J, et al. Vibration damping properties of steel/rubber/composite hybrid structures. *Compos Struct* 2012;94(11):3327–35. <http://dx.doi.org/10.1016/j.compstruct.2012.04.035>.
- [12] Reddy JN. *Mechanics of laminated composite plates and shells*. Boca Raton, FL: CRC Press; 2004, p. 831. <http://dx.doi.org/10.1201/b12409>.
- [13] Carrera E. Theories and finite elements for multilayered plates and shells: A unified compact formulation with numerical assessment and benchmarking. *Arch Comput Methods Eng* 2003;10(3):215–96. <http://dx.doi.org/10.1007/BF02736224>.
- [14] Carrera E, Brischetto S. A survey with numerical assessment of classical and refined theories for the analysis of sandwich plates. *Appl. Mech. Rev.* 2009;62(1):1–17. <http://dx.doi.org/10.1115/1.3013824>.
- [15] Wetzel A, Kärger L, Rolfes R, Rohwer K. Evaluation of two finite element formulations for a rapid 3D stress analysis of sandwich structures. *Comput Struct* 2005;83(19–20):1537–45. <http://dx.doi.org/10.1016/j.compstruct.2005.02.005>.
- [16] Kärger L, Wetzel A, Rolfes R, Rohwer K. A three-layered sandwich element with improved transverse shear stiffness and stresses based on FSDT. *Comput Struct* 2006;84(13–14):843–54. <http://dx.doi.org/10.1016/j.compstruct.2006.02.007>.
- [17] Carrera E. CZ<sup>2</sup> Requirements - models for the two dimensional analysis of multilayered structures. *Compos Struct* 1997;37(3–4):373–83. [http://dx.doi.org/10.1016/S0263-8223\(98\)80005-6](http://dx.doi.org/10.1016/S0263-8223(98)80005-6).
- [18] Carrera E, Ciuffreda A. A unified formulation to assess theories of multilayered plates for various bending problems. *Compos Struct* 2005;69(3):271–93. <http://dx.doi.org/10.1016/j.compstruct.2004.07.003>.
- [19] Carrera E, Cinefra M, Zappino E, Petrolo M. Finite element analysis of structures through unified formulation. *Finite elem. anal. struct. through unified formul.*, vol. 9781119941. Chichester, UK: John Wiley & Sons, Ltd; 2014, p. 1–385. <http://dx.doi.org/10.1002/9781118536643>.
- [20] Demasi L.  $\infty^6$  Mixed plate theories based on the generalized unified formulation. Part I: Governing equations. *Compos Struct* 2009;87(1):1–11. <http://dx.doi.org/10.1016/j.compstruct.2008.07.013>.
- [21] Demasi L.  $\infty^6$  Mixed plate theories based on the generalized unified formulation. Part II: Layerwise theories. *Compos Struct* 2009;87(1):12–22. <http://dx.doi.org/10.1016/j.compstruct.2008.07.012>.
- [22] Demasi L.  $\infty^6$  Mixed plate theories based on the generalized unified formulation. Part III: Advanced mixed high order shear deformation theories. *Compos Struct* 2009;87(3):183–94. <http://dx.doi.org/10.1016/j.compstruct.2008.07.011>.
- [23] Demasi L.  $\infty^6$  Mixed plate theories based on the generalized unified formulation. Part IV: Zig-zag theories. *Compos Struct* 2009;87(3):195–205. <http://dx.doi.org/10.1016/j.compstruct.2008.07.010>.
- [24] Demasi L.  $\infty^6$  Mixed plate theories based on the generalized unified formulation. Part V: Results. *Compos Struct* 2009;88(1):1–16. <http://dx.doi.org/10.1016/j.compstruct.2008.07.009>.
- [25] Carrera E, Petrolo M. Guidelines and recommendations to construct theories for metallic and composite plates. *Am Inst Aeronaut Astronaut* 2010;48(12):2852–66. <http://dx.doi.org/10.2514/1.J050316>.
- [26] Carrera E, Petrolo M. On the effectiveness of higher-order terms in refined beam theories. *J Appl Mech Trans ASME* 2011;78(2). <http://dx.doi.org/10.1115/1.4002207>.
- [27] Carrera E, Miglioretti F, Petrolo M. Computations and evaluations of higher-order theories for free vibration analysis of beams. *J Sound Vib* 2012;331(19):4269–84. <http://dx.doi.org/10.1016/j.jsv.2012.04.017>.
- [28] Petrolo M, Cinefra M, Lamberti A, Carrera E. Evaluation of mixed theories for laminated plates through the axiomatic/asymptotic method. *Composites B* 2015;76:260–72. <http://dx.doi.org/10.1016/j.compositesb.2015.02.027>.
- [29] Jackstadt A, Liebig WV, Sessner V, Weidenmann KA, Kärger L. Application of a mixed variational higher order plate theory towards understanding the deformation behavior of hybrid laminates. *PAMM* 2019;19(1):e201900048. <http://dx.doi.org/10.1002/pamm.201900048>.
- [30] D'Ottavio M. A sublaminar generalized unified formulation for the analysis of composite structures. *Compos Struct* 2016;142:187–99. <http://dx.doi.org/10.1016/j.compstruct.2016.01.087>.
- [31] Carrera E. Layer-wise mixed models for accurate vibrations analysis of multilayered plate. *J Appl Mech Trans ASME* 1998;65(4):820–8. <http://dx.doi.org/10.1115/1.2791917>.
- [32] Carrera E. A Reissner's mixed variational theorem applied to vibration analysis of multilayered shell. *J Appl Mech Trans ASME* 1999;66(1):69–78. <http://dx.doi.org/10.1115/1.2789171>.
- [33] Qatu MS, Sullivan RW, Wang W. Recent research advances on the dynamic analysis of composite shells: 2000–2009. *Compos Struct* 2010;93(1):14–31. <http://dx.doi.org/10.1016/j.compstruct.2010.05.014>.
- [34] Sayyad AS, Ghugal YM. On the free vibration analysis of laminated composite and sandwich plates: A review of recent literature with some numerical results. *Compos Struct* 2015;129:177–201. <http://dx.doi.org/10.1016/j.compstruct.2015.04.007>.
- [35] Ross D, Ungar EE, Kerwin EM. Damping of plate flexural vibrations by means of viscoelastic laminae. In: Ruzicka JE, editor. *Struct. damping*. New York: Pergamon Press; 1960, p. 49–87.
- [36] Rao MD, He S. Dynamic analysis and design of laminated composite beams with multiple damping layers. *Am Inst Aeronaut Astronaut* 1993;31(4):736–45. <http://dx.doi.org/10.2514/3.11611>.
- [37] Ganapathi M, Patel BP, Boisse P, Polit O. Flexural loss factors of sandwich and laminated composite beams using linear and nonlinear dynamic analysis. *Composites B* 1999;30(3):245–56. [http://dx.doi.org/10.1016/S1359-8368\(98\)00063-8](http://dx.doi.org/10.1016/S1359-8368(98)00063-8).
- [38] Xie Z, Shepard WS. An enhanced beam model for constrained layer damping and a parameter study of damping contribution. *J Sound Vib* 2009;319(3–5):1271–84. <http://dx.doi.org/10.1016/j.jsv.2008.06.041>.
- [39] Gupta A, Reddy RS, Panda S, Kumar N. Damping treatment of beam with unconstrained/constrained 1-3 smart viscoelastic composite layer. *Mater Today Proc* 2020;26:956–62. <http://dx.doi.org/10.1016/j.matpr.2020.01.154>.
- [40] Johnson CD, Kienholz DA. Finite element prediction of damping in structures with constrained viscoelastic layers. *Am Inst Aeronaut Astronaut* 1982;20(9):1284–90. <http://dx.doi.org/10.2514/3.51190>.
- [41] Rikards R, Chate A, Barkanov E. Finite element analysis of damping the vibrations of laminated composites. *Comput Struct* 1993;47(6):1005–15. [http://dx.doi.org/10.1016/0045-7949\(93\)90305-W](http://dx.doi.org/10.1016/0045-7949(93)90305-W).
- [42] Moreira RA, Rodrigues JD, Ferreira AJ. A generalized layerwise finite element for multi-layer damping treatments. *Comput Mech* 2006;37(5):426–44. <http://dx.doi.org/10.1007/s00466-005-0714-1>.
- [43] Plagianakos TS, Saravanos DA. High-order layerwise finite element for the damped free-vibration response of thick composite and sandwich composite plates. *Internat J Numer Methods Engrg* 2009;77(11):1593–626. <http://dx.doi.org/10.1002/nme.2465>.
- [44] Akoussan K, Boudaoud H, El-Mostafa D, Carrera E. Vibration modeling of multilayer composite structures with viscoelastic layers. *Mech Adv Mater Struct* 2015;22(1–2):136–49. <http://dx.doi.org/10.1080/15376494.2014.907951>.
- [45] Ren S, Zhao G, Zhang S. A layerwise finite element formulation for vibration and damping analysis of sandwich plate with moderately thick viscoelastic core. *Mech Adv Mater Struct* 2020;27(14):1201–12. <http://dx.doi.org/10.1080/15376494.2018.1504360>.
- [46] Filippi M, Carrera E, Valvano S. Analysis of multilayered structures embedding viscoelastic layers by higher-order, and zig-zag plate elements. *Composites B* 2018;154(May):77–89. <http://dx.doi.org/10.1016/j.compositesb.2018.07.054>.
- [47] Ribeiro ML, Ferreira GF, de Medeiros R, Ferreira AJ, Tita V. Experimental and numerical dynamic analysis of laminate plates via carrera unified formulation. *Compos Struct* 2018;202(May):1176–85. <http://dx.doi.org/10.1016/j.compstruct.2018.05.085>.
- [48] Saravanos DA, Pereira JM. Effects of interply damping layers on the dynamic characteristics of composite plates. *Am Inst Aeronaut Astronaut* 1992;30(12):2906–13. <http://dx.doi.org/10.2514/3.11636>.
- [49] Li J, Narita Y. Analysis and optimal design for the damping property of laminated viscoelastic plates under general edge conditions. *Composites B* 2013;45(1):972–80. <http://dx.doi.org/10.1016/j.compositesb.2012.09.014>.
- [50] Alaimo A, Orlando C, Valvano S. Analytical frequency response solution for composite plates embedding viscoelastic layers. *Aerosp Sci Technol* 2019;92:429–45. <http://dx.doi.org/10.1016/j.ast.2019.06.021>.
- [51] Valvano S, Alaimo A, Orlando C. Analytical analysis of sound transmission in passive damped multilayered shells. *Compos Struct* 2020;253(April):112742. <http://dx.doi.org/10.1016/j.compstruct.2020.112742>.
- [52] Wang S, Zhang J, Li Q, Su J, Liang S. Free vibration of co-cured composite structures with different numbers of viscoelastic damping membranes. *Compos Struct* 2020;247(April):112434. <http://dx.doi.org/10.1016/j.compstruct.2020.112434>.

- [53] Li H, Wang Z, Lv H, Zhou Z, Han Q, Liu J, et al. Nonlinear vibration analysis of fiber reinforced composite cylindrical shells with partial constrained layer damping treatment. *Thin-Walled Struct* 2020;157(August):107000. <http://dx.doi.org/10.1016/j.tws.2020.107000>.
- [54] Li H, Wang W, Wang X, Han Q, Liu J, Qin Z, et al. A nonlinear analytical model of composite plate structure with an mre function layer considering internal magnetic and temperature fields. *Compos Sci Technol* 2020;200(September):108445. <http://dx.doi.org/10.1016/j.compscitech.2020.108445>.
- [55] Jackstadt A, Kärger L. Extension of an analytical solution of a unified formulation to the frequency response of composite plates with viscoelastic layers. *PAMM* 2021;20(1):1–4. <http://dx.doi.org/10.1002/pamm.202000234>.
- [56] D'Ottavio M, Krasnobrizha A, Valot E, Polit O, Vescovini R, Dozio L. Dynamic response of viscoelastic multiple-core sandwich structures. *J Sound Vib* 2021;491(xxxx):115753. <http://dx.doi.org/10.1016/j.jsv.2020.115753>.
- [57] Sessner V. Charakterisierung und Modellierung des Dämpfungsverhaltens von hybriden Faser-Metall-Elastomer-Laminaten (Dissertation), Karlsruher Institut für Technologie (KIT); 2021, <http://dx.doi.org/10.5445/IR/1000130285>.
- [58] Reissner E. On a certain mixed variational theorem and a proposed application. *Internat J Numer Methods Engrg* 1984;20(7):1366–8. <http://dx.doi.org/10.1002/nme.1620200714>.